MITIGATION OF SIGNAL BIASES INTRODUCED BY CONTROLLED RECEPTION PATTERN ANTENNAS IN A HIGH INTEGRITY CARRIER PHASE DIFFERENTIAL GPS SYSTEM

A DISSERTATION

SUBMITTED TO THE DEPARTMENT OF AERONAUTICS AND

ASTRONAUTICS

AND THE COMMITTEE ON GRADUATE STUDIES

OF STANFORD UNIVERSITY

IN PARTIAL FULFILLMENT OF THE REQUIREMENTS FOR THE DEGREE OF

DOCTOR OF PHILOSOPHY

Ung Suok Kim

March 2007

I certify that I have read this dissertation and that in my opinion it is fully adequate, in scope and quality, as dissertation for the degree of Doctor of Philosophy.

_____
Per K. Enge
Principal Advisor

I certify that I have read this dissertation and that in my opinion it is fully adequate, in scope and quality, as dissertation for the degree of Doctor of Philosophy.

_____
Sanjay Lall

I certify that I have read this dissertation and that in my opinion it is fully adequate, in scope and quality, as dissertation for the degree of Doctor of Philosophy.

_____
Matthew West

Approved for the University Committee on Graduate Studies

ABSTRACT

This dissertation characterizes the signal biases seen in Controlled Reception Pattern Antennas (CRPAs) and introduces mitigation schemes for undoing those biases. A CRPA is an array of GPS antennas whose received signals are phased and combined to alter the reception gain pattern of the antenna. It has great benefits in rejecting multipath and RFI. However, CRPAs have not been considered for a carrier phase system before this work, and its exact effect on the received GPS signal measurements has not been studied in depth. Individual antenna elements have some received carrier phase variation according to the incident signal direction. The frequency response of the antennas also introduces a similar variation in the received code phase of the GPS signal. When these antennas are populated in an array, mutual coupling between the elements causes the code and carrier phase patterns to alter for each element. For a high-accuracy high-integrity carrier phase differential GPS system, all such effects on the measured GPS signal are undesirable.

One such system for which CRPAs are being considered is the Joint Precision Approach and Landing System (JPALS). The navy variant of JPALS is called Sea-based JPALS, and its ultimate goal is to facilitate automatic landings of aircraft onto aircraft carriers, even in zero visibility conditions. The aircraft carrier is a very challenging multipath (reflected GPS signals) environment. On top of all this, service must be provided even in the presence of hostile RFI. This makes CRPAs greatly desirable for this program. However, the signal biases introduced by CRPAs must be characterized and removed.

This dissertation presents a characterization of the code and carrier phase biases introduced by CRPA antenna hardware, two distinct mitigation schemes for removing these biases from the CRPA output signal, and an error-bound analysis for

CRPA implementation in a high-integrity carrier phase differential system such as JPALS. The results will show that a compensation scheme is required, in addition to some implementation requirements (unit-by-unit calibration data, temperature controlled CRPA), in order to successfully apply CRPAs to JPALS and correctly solve the integer ambiguity problem.

ACKNOWLEDGMENTS

The completion of the research for this dissertation would not have been possible without the help and support of many people, to whom I owe a debt of gratitude. First of all, I would like to thank my principal research advisor, Professor Per Enge, for providing me the opportunity to work in the Stanford GPS Laboratory. Through difficult times, he has provided steadfast guidance and support, not only for my academic research, but also in my personal life. I will always be grateful for his continued confidence in me, and I consider it a blessing to have met and worked with such a wonderful advisor.

I would also like to thank my dissertation reading committee members, Professor Sanjay Lall and Professor Matthew West, who were also gracious enough to be on my defense committee. Their valuable suggestions, insights, and probing inquiries provided great guidance in putting together this manuscript.

Special thanks is offered to Professor John Orr of Worcester Polytechnic Institute, who during his sabbatical stay at the Stanford GPS Lab, provided invaluable expertise and advise to lay the foundation for the research presented here, and to Dr. Changdon Kee of Seoul National University for your continued interest and guidance in my work.

I would also like to extend my gratitude to Professor Chris Bartone and Mr. Ian Barton of the Ohio University Avionics Engineering Center (AEC), for providing generous access to their superb anechoic chamber facilities, and for the technical support during data collection scans.

I would like to thank my friends and colleagues in the Stanford GPS Laboratory, without a doubt a collection of the most brilliant minds I have ever had the privilege of being around. Thanks go to Lee Boyce, Juyong Do, Chad Jennings,

Eui-ho Kim, Sherman Lo, and Jiwon Seo for their friendship and support. Special mention is needed for my fellow JPALS research teammates, Tsung Yu Chiou, Mike Koenig, and Dave DeLorenzo, as well as current and past program managers Dr. Jason Rife, Dr. Jenny Gautier, Dr. Dennis Akos, and Dr. Demoz Gebre-Egziahber. I would also like to thank the JPALS program office and the Naval Air Warfare Center Aircraft Division for their generous funding of this research through contract N00421-05-C-0068.

Last but not least, I would like to thank my mom and dad, for their endless sacrifice and love in supporting me throughout my life, and to my brother for the much needed light hearted conversations. Finally, I would like to send my love and gratitude to my wife and my beautiful daughter. It is to my family that I dedicate this dissertation.

TABLE OF CONTENTS

LIST OF TABLES

Number *Page*

LIST OF FIGURES

Number *Page*

LIST OF ACRONYMS

AE	Antenna Electronics
CRPA	Controlled Reception Pattern Antenna
CW	Continuous Wave
DBF	Deterministic Beam Forming
DGPS	Differential GPS
DoD	Department of Defense
FFT	Fast Fourier Transform
GPS	Global Positioning System
HFSS	High Frequency Structure Simulator
IFFT	Inverse Fast Fourier Transform
JPALS	Joint Precision Approach and Landing System
Mcps	Mega-chips per second
MCS	Master Control Station
Pr(false alarm)	Probability of False Alarm
Pr(HMI)	Probability of Hazardously Misleading Information
PRN	Pseudo Random Noise
RF	Radio Frequency
RFI	Radio Frequency Interference
RHCP	Right Hand Circularly Polarized
SFAP	Space Frequency Adaptive Processing
STAP	Space Time Adaptive Processing
TOA	Time of arrival
VAL	Vertical Alarm Limit

CHAPTER 1: INTRODUCTION

1.1 THE GLOBAL POSITIONING SYSTEM

The Global Positioning System (GPS) is a space based radio navigation system that provides 3D positioning and timing solutions to users anywhere in the world at any time of the day. Civilian GPS signals are free for everyone to use and recent advancements in the cost and size of GPS receiver hardware has lead to an immense surge in the usage of GPS. GPS provides personal navigation and is widely used by motorists, hikers, marine enthusiasts, and aviators. It has also found its way into critical uses in the timing community, and provides low-cost synchronization of time-based systems such as cellular phone networks. Today, GPS use has become integrated in our everyday lives, and the world is a much more convenient place for it.

The wide popularity of GPS has also exposed areas of needed improvement. These range from improved availability and increased coverage in urban canyons and indoor environments, to increased accuracy for high precision applications. In an effort to address these issues and to improve service, second and third civil frequencies are being added which will significantly improve the accuracy and availability of GPS. Also, the upcoming Galileo system, a GPS-like counterpart that is being fielded by the European Union, will enable new levels of service as hardware manufacturers take advantage of these multiple frequency options.

1.1.1 GPS System Architecture

GPS consists of three major segments: the Control Segment, the User Segment, and the Space Segment. The Space Segment includes the GPS satellites in orbit around Earth. The Control Segment is responsible for monitoring and maintaining the health of these satellites. Both the Space Segment and the Control Segment are under the control of the U.S. Department of Defense (DoD). The User Segment includes all the user equipment serving a great breadth of military and civilian applications [Enge].

1.1.1.1 The Space Segment

As stated, the Space Segment is comprised of the GPS satellites in orbit around Earth. Currently, the baseline constellation consists of 24 satellites, in near circular orbits with a period of about 12 hours in stationary ground tracks. These orbits are called MEOs (Medium Earth Orbits) and are in six separate orbital planes, all inclined at 55 degrees relative to the equatorial plane (see Figure 1-1). The system can support up to thirty satellites in orbit. Although the base constellation consists of 24 satellites, as of October 2006, there are 30 GPS satellites in orbit. As these satellites age and fail, the DoD plans to upgrade them with satellites carrying the new signals. The DoD plans to maintain and upgrade a full constellation of GPS satellites well into the future [Bauer].

Figure 1-1. GPS Space Segment (picture courtesy of www.nasm.si.edu/gps/)

1.1.1.2 The Control Segment

The Control Segment monitors and maintains the health of the Space Segment. There are a number of monitor stations located around the globe which keep a constant watch on the GPS satellites. These monitor stations are located in Ascension Island, Diego Garcia, Kwajalein, Hawaii, Cape Canaveral and Colorado Springs. The monitor stations are operated remotely by the Master Control Station (MCS), which is located at the Schriever Air Force Base near Colorado Springs, Colorado. Any required communications to the GPS satellites are made via S-band radio link ground antennas co-located with monitor stations at Ascension Island, Cape Canaveral, Diego Garcia, and Kwajalein. The specific functions of the Control Segment are to :

- Monitor satellite orbits,
- Monitor and maintain satellite health,
- Maintain GPS time,
- Predict satellite ephemerides and clock parameters,
- Update satellite navigation messages, and
- Command small thrust maneuvers to maintain orbit or relocate satellites to compensate for failures as required.

The Control Segment maintains the ability to monitor and communicate with the entire GPS constellation at all times with their multiple monitoring stations and ground antennas located throughout the world.

1.1.1.3 The User Segment

The User Segment consists of the GPS receiver equipment that is used to receive and calculate position/time solutions from the GPS signals. This particular segment has seen explosive growth over the past couple of decades in the civil sector. This growth directly coincides with the advancements in integrated circuits, which allowed GPS receivers to be smaller, lighter, and less expensive. This not only made GPS receivers more readily available, it also led to more integration of GPS hardware into other consumer electronic products. Today, many cellular phones come equipped

with GPS receivers which allow 911 emergency personnel to locate where a call is coming from, and in certain products, provides personal navigation services. The User Segment continues to grow, presenting new applications and uses for GPS, both in the military and civil sectors.

1.1.2 GPS SIGNAL STRUCTURE

Currently, GPS signals are transmitted on two separate radio frequencies in the L-band, referred to as L1 and L2. The center frequencies for L1 and L2 are as follows.

$$\text{L1} : f_{\text{L1}} = 1575.42 \text{ MHz} \qquad \text{L2} : f_{\text{L2}} = 1227.60 \text{ MHz}$$

There are two signals transmitted on L1. One is for civilian use, and the other is for DoD authorized users and is encrypted. The signal transmitted on L2 is principally for DoD authorized users and is also encrypted. Civilians are allowed access to the L2 signal, but without explicit knowledge of the ranging codes. Each signal consists of the following three components.

- *Carrier* : RF sinusoidal signal with frequency of f_{L1} or f_{L2}.
- *Ranging Code* : a unique sequence of 0s and 1s assigned to each satellite that modulate the underlying carrier signal. These sequences allow the receiver to determine the signal transit time between transmit and receive instantaneously, and are called

pseudo-random noise (PRN) codes. The codes possess cross correlation properties that allow all the satellites to transmit the carrier wave at the same frequency without the signals interfering with each other. Each satellite transmits two different codes: a civilian course acquisition C/A code, and a precision encrypted P(Y) code. The C/A code is a unique sequence of 1023 bits or chips, repeating every millisecond, which results in a chip width, or wavelength, of 300 meters. The rate of the C/A code chips, called the chipping rate, is 1.023 megachips/sec (Mcps). The P(Y) code sequence is a much longer sequence of chips whose chipping rate is 10.23 Mcps (ten times that of C/A codes). The Y codes are encrypted versions of the P codes, and overall L2 combination is referred to as the P(Y) code. The chip width (wavelength) for P(Y) codes is 30 meters, and leads to greater precision in range measurements than C/A codes.

- *Navigation Data* : a binary-coded message that consists of data on the satellite health, satellite position and velocity (ephemeris), clock bias parameters, and an almanac that gives ephemeris data on all the satellites in the GPS constellation. This binary code modulates the PRN code modulated carrier signal. This message is transmitted at a much slower rate, 50 bits per second (bps). It takes 12.5

minutes to receive the entire message. Please see Figure 1-2 below for a graphical representation of these signal components.

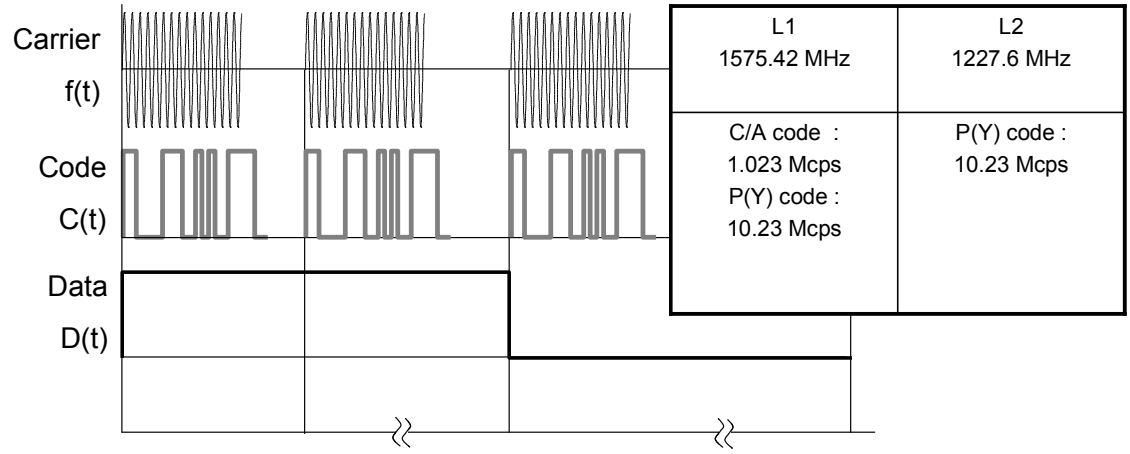

$$s^{(k)}(t) = \sqrt{2P_C}\,C_{C/A}^{(k)}(t)D^{(k)}(t)\sin(2\pi f_{L1}t + \theta_{L1}) + \sqrt{2P_{P(Y),L1}}\,C_{P(Y)}^{(k)}(t)D^{(k)}(t)\cos(2\pi f_{L1}t + \theta_{L1})$$
$$+ \sqrt{2P_{P(Y),L2}}\,C_{Y}^{(k)}(t)D^{(k)}(t)\sin(2\pi f_{L2}t + \theta_{L2}) \qquad \text{Eqn (1-1)}$$

Figure 1-2. GPS Signal Components

Equation (1-1) represents the signal that is transmitted from each satellite k. Each satellite radiates three separate signals: C/A coded signal at L1, P(Y) coded signal at L1, and a P(Y) coded signal at L2 [Enge].

1.1.2.1 GPS Position Solution

GPS uses time-of-arrival (TOA) measurements to determine the range to each satellite, and it uses multi-lateration to pinpoint the location of the user. The carefully chosen PRN code sequence allows the measurement of the transit time of the GPS

signal from satellite transmit to user receipt. This is physically done by measuring the time shift required to align a replica PRN code sequence generated at the receiver with the received signal from the satellite. This transit time is in direct proportion with the range between the satellite and the user, and this determined range is dubbed a pseudorange. Also, the precise location of the transmitting satellites can be determined from the navigation data that is received from each satellite. With the known satellite locations and the range to those satellites, multi-lateration can be used to pinpoint the 3D location of the user. A minimum of four satellite signals must be received and tracked properly to solve for four unknown variables. Three of these unknown variables correspond to the 3D location of the user. The fourth unknown variable is the receiver clock bias, and it arises because the user receiver clock is not synchronized with the GPS system clock. Because the pseudorange is based on signal transit time measurements, this clock bias plays a big role in determining the exact position solution. Only three satellite signals are required for a 2D position solution (no altitude information) [Kaplan].

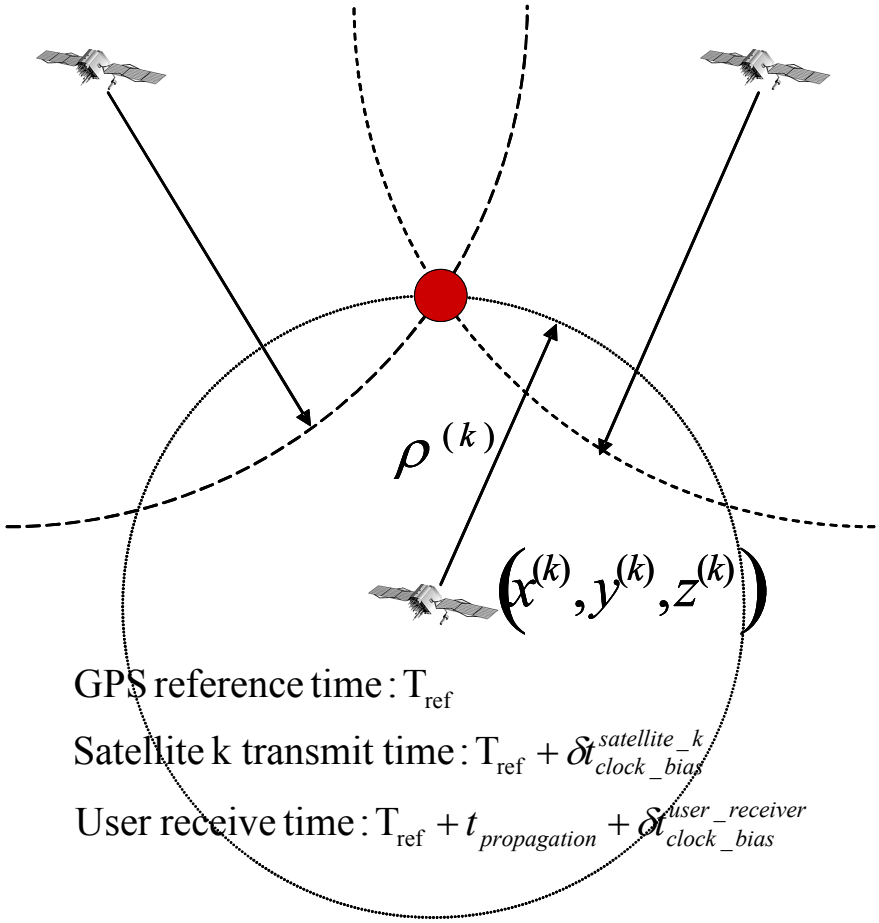

Figure 1-3. Trilateration Using Pseudoranges to Determine Position

1.1.2.2 Measurement Models

The measured pseudorange and carrier phase of the signal received from the satellites can be written as follows.

$$\rho = r + c[\delta t_u - \delta t^s] + I_\rho + T_\rho + \varepsilon_\rho$$
$$\phi = \lambda^{-1}[r + I_\phi + T_\phi] + \frac{c}{\lambda}(\delta t_u - \delta t^s) + N + \varepsilon_\phi \qquad \text{Eqn (1-2)}$$

where

ρ = pseudorange r = actual range
c = speed of light in vacuum δt_u = user clock bias
δt^s = satellite clock bias I = Ionosphere delay
T = Troposphere delay ϕ = carrier phase measurement
λ = carrier wavelength N = unknown integer cycles
ε = random noise

For a more detailed breakdown of each term and the derivation of the above measurement equations, please refer to [Enge]. As can be seen in the above breakdown, the measurements contain nuisance parameters and error sources. These include: differences in the clock biases between the user and the satellite, additional delays caused by the radio signal propagating through the ionosphere and troposphere, and background thermal noise. For the carrier phase measurement, an additional unknown integer cycle term between the user and the satellite is present, which must be resolved for the carrier phase measurement to provide a range solution. Both measurements also contain an error due to thermal noise.

1.1.3 CARRIER PHASE DIFFERENTIAL GPS

Carrier Phase Differential GPS provides high precision relative positioning between a reference receiver and the user, and is particularly important to this dissertation. It is based on the assumption that the baseline (distance between user and reference) is small enough that the line-of-sights from the user and the reference to the satellite can be considered the same. In addition, the ionosphere and the troposphere delays seen by the reference and user are nearly identical. If these assumptions are accurate, then the carrier phase measurement taken by the reference antenna and the user antenna can be differenced to remove the common mode error terms present in both measurements. Equation (1-3) listed in Figure 1-4 below is the received carrier phase component of Equation (1-2). Equation (1-4) shows the differenced carrier phase measurement that shows the common mode errors removed. The subscript in each term refers to the differenced sources (u for user and r for reference). This differenced measurement can act as an ultra-precise range measurement between the user and reference. In order for the differenced carrier phase measurement to be used as a range measurement, the unknown integer number of cycles must be resolved [Parkinson].

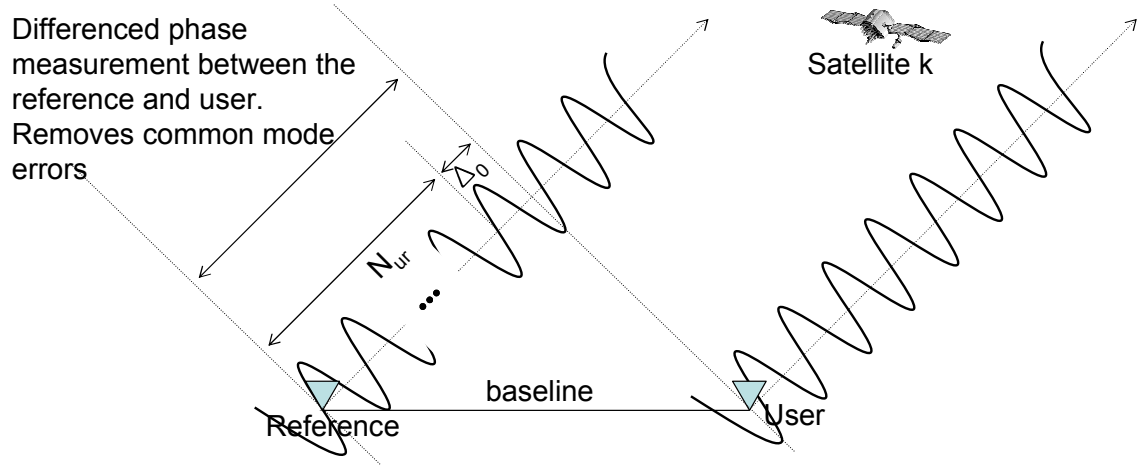

$$\phi_u^{(k)} = \lambda^{-1}\left[r_u^{(k)} - I_u^{(k)} + T_u^{(k)}\right] + f\left(\delta t_u - \delta t^{(k)}\right) + N_u^{(k)} + \varepsilon_{\phi,u}^{(k)} \quad \text{Eqn (1-3)}$$

$$\phi_{ur}^{(k)} = \lambda^{-1} r_{ur}^{(k)} + f\delta t_{ur} + N_{ur}^{(k)} + \varepsilon_{\phi,ur}^{(k)} \quad \text{Eqn (1-4)}$$

Figure 1-4. Carrier Phase Differential GPS

1.1.3.1 Single Differenced Carrier Measurement

As can be seen from Equation (1-4), the single difference carrier measurement has eliminated (or nearly so) the ionosphere and troposphere delays. These two error sources were assumed to be identical between the user and the reference and thus can be removed by differencing the two measurements. However, the single difference still contains the difference in the clock bias between the user and the reference receivers. A second difference removes this nuisance parameter. This is called double differencing.

1.1.3.2 Double Differenced Carrier Measurement

Double differencing removes the clock bias in the single differenced carrier phase range equation. First, a reference satellite k is chosen (the choice of satellite can be arbitrary, but the highest elevation satellite is usually chosen). Then, all of the other single differenced carrier measurements from each satellite are differenced with this satellite k single differenced carrier measurement. The result is a double difference carrier phase measurement between the user and the reference receivers and between satellites, and the troublesome clock bias term drops out. Now the only remaining bias is the double differenced integer cycles, and there are numerous methods for treating this term.

One such technique by which the unknown integer cycles are solved involves an exhaustive search over a given search space of possible integer candidates [Parkinson]. First, a set of candidate integer ambiguities are generated based on the initial position estimate and its associated uncertainty. Next, all of the possible integer ambiguity combinations are evaluated according to a specific error cost function, and the integer set returning the lowest cost function value is chosen as the solution. A straight forward application of the above method results in a very large search space. The double differenced measurements are unfortunately highly correlated and result in very thin elongated search spaces, leading to long search times. One method for dealing with this is called LAMBDA (Lease-squares Ambiguity Decorrelation Adjustment), which decorrelates each double differenced measurement and results in a much more manageable search space [Teunissen].

As mentioned, there are many different methods for solving the integer ambiguity problem. Those methods are beyond the scope of this dissertation. For a more detailed in-depth investigation of integer ambiguity resolution, please refer to [Teunissen], [Parkinson], and [Hein]. However, keep in mind that this integer ambiguity problem must be resolved in order to obtain relative position solution from these differenced carrier phase measurements, and this will be at the heart of all subsequent research presented in this dissertation.

1.2 JOINT PRECISION APPROACH AND LANDING SYSTEM

The Joint Precision Approach and Landing System (JPALS) is a system being developed by the U.S Department of Defense to provide navigation for the landing of U.S. military aircraft. JPALS is a very broad and multi-discipline program that encompasses a number of different usage scenarios. Broadly, it can be broken down into two separate categories: Land based JPALS and Sea based JPALS. Land based JPALS will be predominantly used for fixed installations and airfields, although a special operations scenario is being investigated for a quick, field-operable landing navigation system. Sea based JPALS will be for the landing of different types of aircraft onto U.S. Navy aircraft carriers [Peterson 05]. For both implementations, GPS will be the primary source of navigation information. Each implementation has unique challenges and environments, and many advanced technologies are being considered

for implementation. However, Sea based JPALS is the more challenging of the two, and is the primary focus of this dissertation.

As stated, Sea based JPALS is being developed to provide navigation for landing aircraft on aircraft carriers. As one can imagine, carrier landing demands very high accuracy, and Sea based JPALS requires vertical position accuracy to be within 0.2 meters [SRD]. Thus, a dual frequency carrier phase differential GPS system is being pursued. In addition, the navigation solution must have high integrity, and service should not be interrupted, even in the presence of hostile RFI (radio frequency interference). The integrity requirement for this system is one of the key factors that drive the use of advanced technologies in JPALS. Integrity refers to the confidence that can be placed on the validity or the accuracy of the navigation position solutions reported by the system. For aviation applications, this requirement is usually given by the following parameters:

- VAL : The Vertical Alarm Limit, or VAL, specifies a level of position error uncertainty in the vertical direction that can be tolerated before an alarm is raised and the position solution flagged as unsuitable for use. For Sea based JPALS, this value is 1.1 meters. An alarm must be raised any time the uncertainty in the vertical position solution exceeds 1.1 meters.

- Pr(false alarm) : This is a failure of the system VAL requirements. A false alarm occurs when the vertical position uncertainty is

actually within the VAL limit, but an alarm is raised. The probability of this occurring is given by Pr(false alarm), and this affects the availability of the system and the continuity of the position solution provided.

- Pr(HMI) : Perhaps more critical to safety of life is the Probability of Hazardously Misleading Information, Pr(HMI). The second mode of VAL requirement failure occurs when the vertical position uncertainty actually exceeds the VAL limit without an alarm being raised. This failures represents a potential safety risk to the user, and is captured by Pr(HMI). For Sea based JPALS, this probability must be less than 10^{-7} per approach.

- Time-to-alarm : Any alarms that are raised due to the VAL infringement must be raised in a timely manner, giving the user enough time to take note and consider appropriate action. For a highly dynamic application like JPALS, this is especially true, and the time-to-alarm requirement is 1 second.

JPALS, especially Sea based JPALS, is very challenging because of the accuracy and integrity requirements placed on the system. Because of the challenging requirements, current existing implementations of carrier phase DGPS will not be adequate, and advanced technologies must be considered. To specifically meet the challenge of providing service in the presence of hostile RFI, controlled reception

pattern antennas (CRPAs) and their interference rejection capabilities will be required for Sea based JPALS [Peterson 04]. However, CRPAs have never been used for a high precision carrier phase DGPS system before, and their use in such a system presents many difficulties. The main subject of this dissertation is the investigation of the feasibility of implementing CRPAs in Sea based JPALS to take advantage of their interference rejection capabilities, while at the same time maintaining the integrity of the received signal in order to provide high precision navigation solutions based on a differential carrier phase system [Pervan 01].

1.3 CONTROLLED RECEPTION PATTERN ANTENNAS

A Controlled Reception Pattern Antenna (CRPA) is a GPS antenna array that processes signals to provide gain or attenuation in specific directions of interest. A CRPA is a phased array, where each antenna element channel signal is phase shifted and combined to form the phased array output. By adjusting the amount of phase shift in each channel, the signal direction for in-phase or out-of-phase combination can be controlled. When signals combine in-phase, the signal gain in that direction will be increased, while out-of-phase combinations will result in nulls being placed in those directions [Visser].

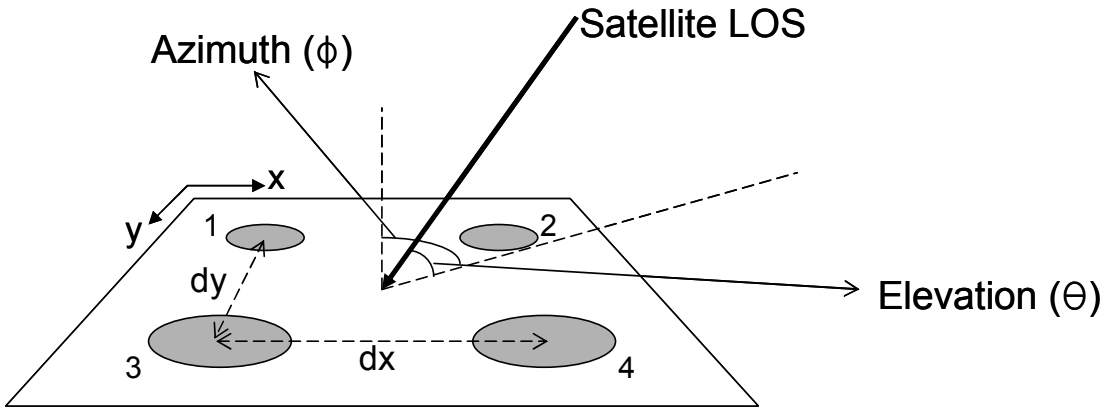

Figure 1-5. 2x2 CRPA implementation

Based on the geometry of the problem shown in Figure 5, the following phase shifts for each channel form a beam in the Θ, ϕ directions (Equation 1-5). The equations below are purely dependent on the geometry of the problem (array baseline length between elements, array orientation, line-of-sight direction to signal) [Balanis].

$$phshift_{x-dir} = \frac{2\pi d_x \cos(\theta)\sin(\phi)}{\lambda}$$
$$phshift_{y-dir} = \frac{2\pi d_y \cos(\theta)\cos(\phi)}{\lambda} \qquad \text{Eqn (1-5)}$$
$$phshift_{xy-dir} = phshift_x + phshift_y$$

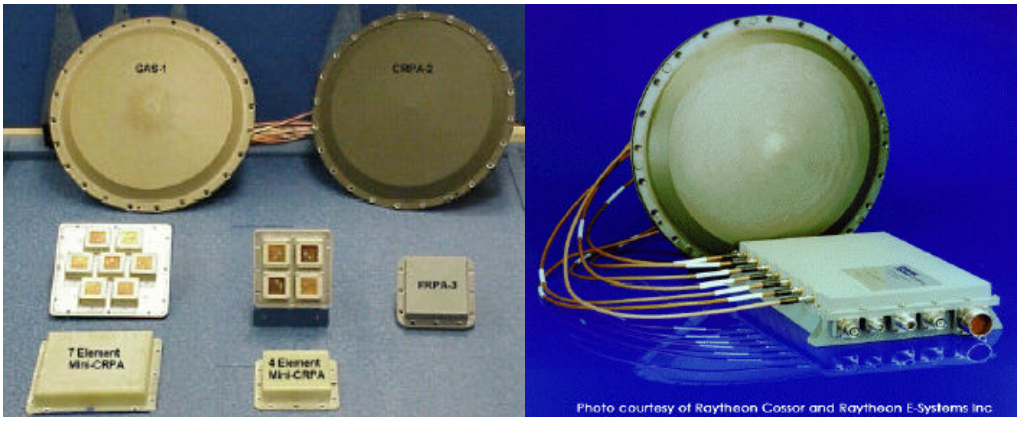

Figure 1-6. CRPAs in use today along with antenna electronics (AE) package

Some typical CRPA hardware are shown in Figure 1-6 above. CRPAs can be broken down into two major components. First, the CRPA array is the physical array of GPS antenna elements. CRPAs have anywhere from 2 to 16 antenna elements, usually spaced by approximately ½ carrier wavelength. The antenna electronics (AE) processes, phase-shifts, and combines these signals to form a single output signal. There are many different algorithms for processing each channel signal, each of which has their specific characteristics. These algorithms are also an active area of research currently at Stanford University and elsewhere for JPALS application. However, for this dissertation, a simple but representative AE algorithm will be chosen to illustrate the biases introduced by the CRPA antenna hardware into the received GPS signal. Also, mitigation schemes will be suggested to undo these biases while being able to enjoy the interference rejection benefits of CRPAs.

As mentioned above, many different algorithms have been proposed to combine the signals from the CRPA elements. Figure 1-7 shows sample gain patterns

for some example algorithms and for a specific set of interference strengths and directions. The antenna used was a seven element hexagonal configuration array with ½ wavelength baselines. The three different algorithms shown are deterministic spatial nulling, STAP (Space Time Adaptive Processing) and SFAP (Space Frequency Adaptive Processing). Please see [Widrow] and [Manolakis] for more in depth coverage of each algorithm. As can be seen from the plots, CRPAs can provide as much as -60 dB of protection against interference sources, and could ensure navigation service in challenging RFI environments. However, the associated biases introduced by CRPAs must be characterized before they can be implemented in Sea based JPALS.

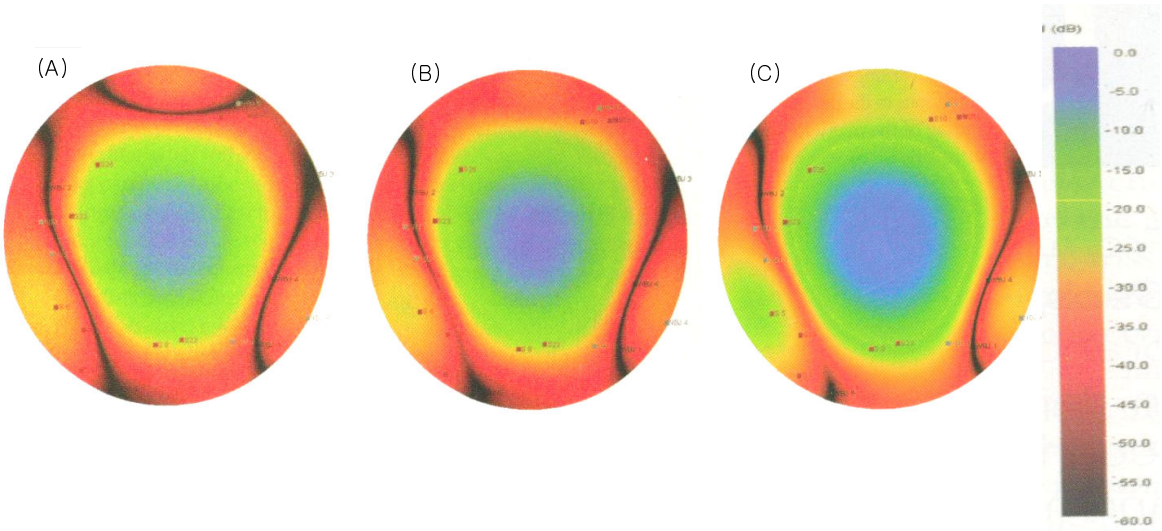

Figure 1-7. Different CRPA algorithms on seven element array: (A) Deterministic Spatial Nulling, (B) Space Temporal Adaptive Processing (STAP), (C) Space Frequency Adaptive Processing (SFAP) [Rounds]

1.4 CONTRIBUTIONS

This dissertation will present an in-depth investigation of the application of CRPA arrays to high-integrity, differential carrier phase GPS systems such as Sea based JPALS. As discussed above, CRPAs mitigate RFI, but they have never been applied in a differential carrier phase system.

The contributions presented in this dissertation can be organized into the following major points.

1. CRPA array hardware effects on the received GPS signal : The effects on the code and carrier phase that are introduced into the received GPS signal by the CRPA array hardware are analyzed and presented.

2. Mitigation schemes for above effects : Two mitigation schemes for undoing the above hardware effects are outlined, and their effectiveness analyzed and presented.

3. Environmental and Manufacturing Tolerance Effects : The environmental effects and manufacturing tolerances on the CRPA array can add additional errors to the mitigation schemes presented. These real world effects are categorized and bounded.

4. Error Budget Investigation : All of the above are combined in an error budget feasibility analysis based on the Sea based JPALS specifications, with the goal of facilitating a successful integer ambiguity resolution. This in turn

illustrates the requirements for CRPA hardware in order for successful implementation in Sea based JPALS.

In order to successfully apply CRPAs to JPALS, we must understand the mutual coupling that occurs between the elements in an antenna array. Mutual coupling affects the received GPS signal structure, right down to and including the code and carrier phase, the accurate measurements of which are critical to a successful navigation system. In order to guarantee accurate carrier phase processing, all facets of CRPAs must be understood, and their use in this new application must be investigated in a manner that has not been documented in prior work [Behre]. This investigation will be the primary focus of this dissertation, and the results will be presented within the context of the Sea based JPALS performance requirement specifications.

Before the above contributions are presented, a more in-depth consideration of single stand-alone microstrip patch antennas is presented in the following chapter. This should provide a good foundation for launching into the above contributions and the analysis of CRPA arrays.

CHAPTER 2: SIGNAL BIASES IN SINGLE MICROSTRIP PATCH ANTENNAS

For aviation GPS applications, microstrip antennas (or patch antennas) have been the antennas of choice primarily due to their small size. Microstrip antennas can be placed on the exterior skin of the aircraft where they have the best line of sight to GPS satellites, while at the same time minimizing additional drag due to their low profile. In addition, patch antennas are easy to manufacture at low cost and are very robust mechanically, allowing them to survive the stressful environment presented by aviation applications [James]. For these reasons, almost all available CRPAs have patch antenna elements, regardless of configuration, number of elements, single or dual frequency implementation, etc.

Unfortunately, patch antennas do suffer some disadvantages. The most relevant to the present work are: low efficiency, small bandwidth, and manufacturing tolerance problems. Low efficiency along with small bandwidth combine to compound mutual coupling related issues for array applications. Small bandwidth, along with the geometry of the patch antenna, leads to direction dependent bias variations. Manufacturing tolerance problems can cause variations in antenna response [James]. This is especially relevant to arrays where multiple antenna elements are closely spaced. These tolerance effects can lead to a unique and differing mutual coupling environment for each CRPA

array. All of the above disadvantages of patch antennas will be presented and analyzed in subsequent chapters, with an emphasis on CRPA use for JPALS.

First, signal biases introduced by microstrip patch antennas are investigated. As we shall discover, these signal biases vary with signal direction and thus must be compensated. Also, the ramifications of these effects in the context of a differential system will be considered. The overall goal of this chapter is to form the foundation and requirements for the CRPA array application in a high integrity, high precision differential GPS system (like JPALS) by first studying a single stand-alone patch antenna.

2.1 PATCH ANTENNAS

Patch antennas consist of a ground plane, with a substrate layer of certain thickness above the ground plane, and a metallic patch of given geometry lying on top (Figure 2-1). Patch antenna performance is determined by: the dielectric properties of the substrate material, the geometry of the patch, and the method of feeding the top patch. There are countless possible geometries for the top patch shape and size (square, rectangular, circular, elliptical, triangle, unconventional, etc). Also, there are numerous possible feed methods to choose from (microstrip line feed, coaxial probe feed, aperture couple feed, proximity couple feed, etc) [Stutzman].

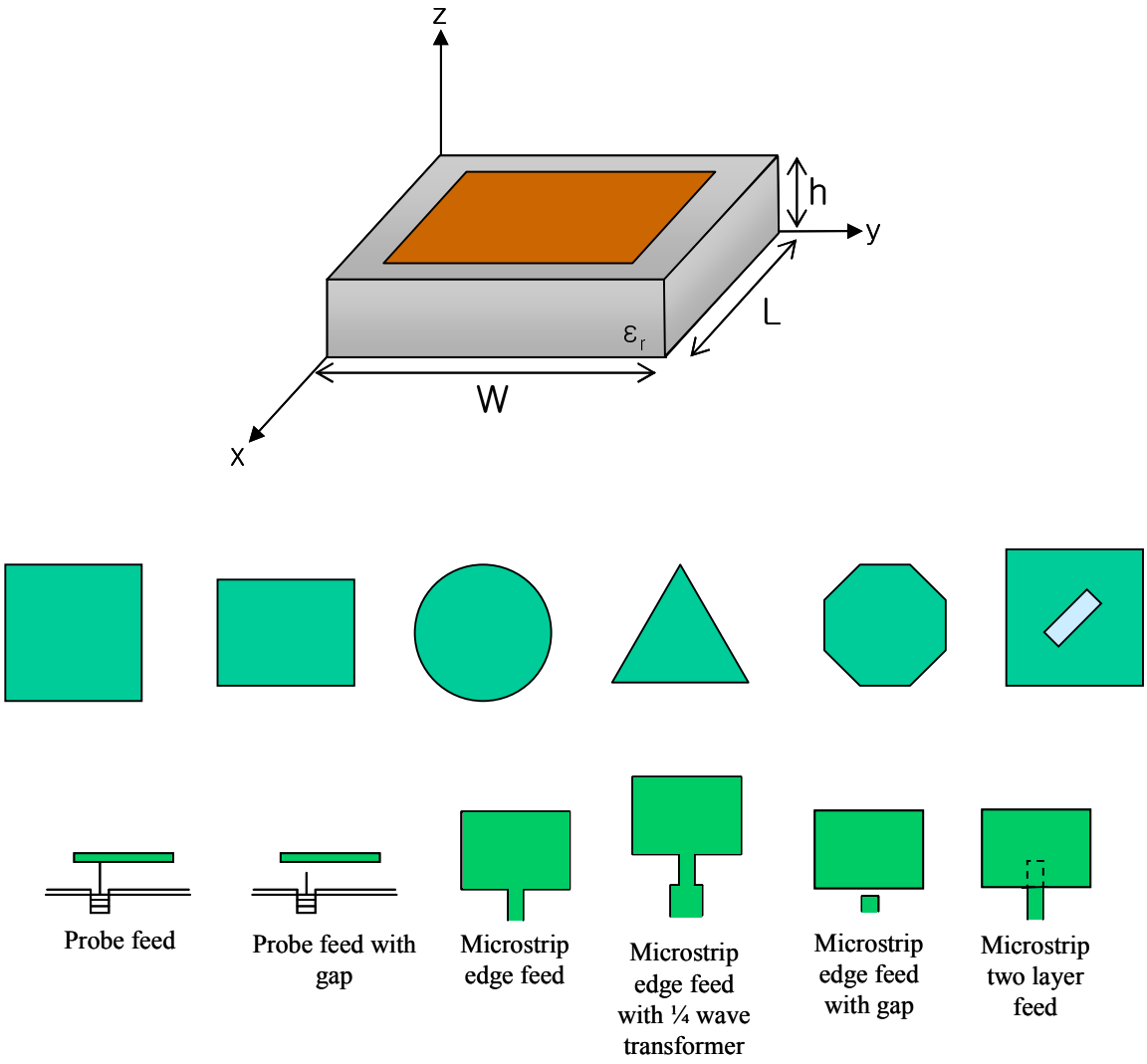

Figure 2-1. Microstrip Antennas (Patch Antenna) : Different Patch Shapes and Feed Methods [Stutzman]

The mechanisms by which patch antennas receive electromagnetic waves from the air are as follows. An incident electromagnetic wave will induce electric fields within the dielectric substrate material. These electric fields will cause electrons to flow on the

top patch. Those electrons that combine at the feed point and travel down the feed line will form the received signal. The impedance of the antenna must closely match that of the line that is connected to the antenna for maximum signal power transfer [Zurcher].

In general, the patch antennas used in CRPAs have relatively simple geometries, so this dissertation will consider rectangular patch antennas fed by a single coaxial probe [Allen].

2.2 REQUIREMENTS FOR CARRIER PHASE DIFFERENTIAL GPS RELATIVE POSITIONING

As mentioned briefly in Chapter 1, the resolution of the integer ambiguity is a critical step in obtaining a high precision relative range signal from the differenced carrier phase measurements. There are numerous methods by which these integer ambiguities are resolved, and most of these involve a time iterative search procedure. As mentioned before, the exact algorithms for the integer ambiguity resolution are beyond the scope of this dissertation. For all of these algorithms, the pseudorange measurements are used as a basis for resolving the carrier phase integer ambiguity. In other words, the first estimate of the integer ambiguity is the pseudorange measurement divided by the carrier wavelength [Parkinson].

Thus, we have two criteria for successful integer ambiguity resolution in the static sense:

- The pseudorange measurement determined from the received code phase must have an error less than 1/2 carrier wavelength. Errors larger than 1/2 wavelength may add ± 1 to the pseudorange based integer determination.

- The carrier phase measurement must have error less than 1/2 carrier wavelength.

Since JPALS is a differential system, the above requirements are placed on the difference of the two code and carrier phase measurements, i.e., reference code minus rover code phase. However, there are other factors that drive this requirement further. Thermal noise is important, as is the fact the integers are being processed dynamically. These requirements on the code and carrier phase errors have been investigated in-depth for the Sea based JPALS requirement. Taking into account the dynamic processing of the integer ambiguities, reference [Pervan 03] determined the required signal errors for Sea based JPALS processing as follows. We will use the below numbers to evaluate CRPA feasibility in this dissertation.

$$\text{error}_{\text{code phase}} < 8 \text{ cm}$$

$$\text{error}_{\text{carrier phase}} < 10 \text{ degrees}$$

2.2.1 DESIGN OF CHOSEN PATCH

The basic design procedure for a rectangular patch will be briefly covered. We need the antenna to be Right Hand Circularly Polarized (RHCP) to receive GPS signals with a simple and repeatable manufacturing process. The starting point for the design is a square patch. First, the dimensions for the square patch must be calculated to fix the center frequency of the antenna based on the dielectric constant and the thickness of the substrate material. To receive RHCP signals, the received signal for the top edge must be 90 degrees ahead in phase of a similar signal received along the right edge [James].

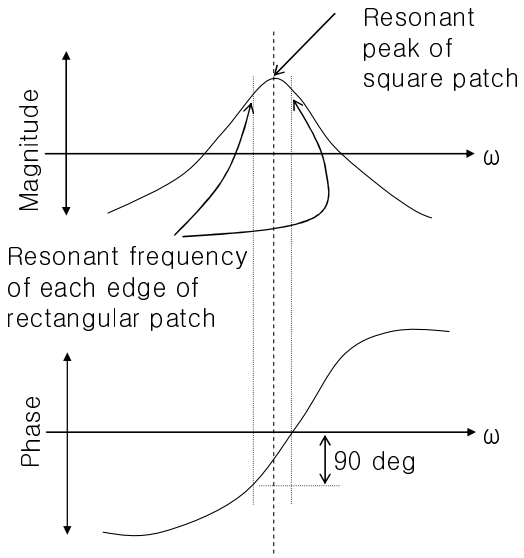

Figure 2-2. Rectangular Patch Tuning Concept: Frequency Response of Square Patch

Consider Figure 2-2 above. The frequency response is representative of a square patch. The goal is to slightly mistune the dimensions on each edge such that the received phase along each edge is equally nudged above and below on the phase response curve,

resulting in it being exactly 90 degrees out of tune. Care must be taken to equalize the mistuning effort along each side to ensure that the center frequency of the antenna is not compromised.

Using a cavity model for the patch antenna where the top patch and bottom ground plane are perfectly conducting electrically and the side walls are perfectly conducting magnetically, we can derive the following from Maxwell's equations [James]:

The vector potential, A, must satisfy

$$\nabla^2 A + k^2 A = 0$$

Applying the appropriate boundary conditions,

$$k_x = \left(\frac{m\pi}{L}\right), m = 0,1,2,...$$

$$k_y = \left(\frac{n\pi}{W}\right), n = 0,1,2,...$$

$$k_z = \left(\frac{p\pi}{h}\right), p = 0,1,2,...$$

$$A = A_{mnp}\cos(k_x x)\cos(k_y y)\cos(k_z z)$$

where

A_{mnp} : amplitude coefficient of each mnp mode

k_x, k_y, k_z : wavenumbers along the x, y and z directions

m, n, p : number of half-cycle field variations along the x,y and z directions

The wave numbers $k_x, k_y,$ and k_z are subject to the following constraint equation

$$k_x^2 + k_y^2 + k_z^2 = k_r^2 = \omega_r^2 \mu\varepsilon$$

and the resonant frequencies for the cavity are given by

$$(f_r)_{mnp} = \frac{c}{2\pi\sqrt{\varepsilon_r}}\sqrt{\left(\frac{m\pi}{L}\right)^2 + \left(\frac{n\pi}{W}\right)^2 + \left(\frac{p\pi}{h}\right)^2}$$

With the above equation, we set $(f_r)_{100} = (f_r)_{010}$ = L1 = 1575.42 MHz and solve for L and W (L=W) to set dimensions for the square patch. The amount of adjustment required in the dimensions along each edge is given by the following.

The quality factor, Q_t, is representative of antenna losses.

$$Q_t \approx \frac{\omega \varepsilon_r L^2}{2hG_{rad}}$$

where G_{rad} is the radiation conductance and is approximated by

$$G_{rad} \approx \frac{L}{120\lambda_0}\left[1 - \frac{1}{24}\left(\frac{\omega h}{c}\right)^2\right]$$

To achieve circular polarization, the axial ratio at broadside of the E_x to the E_y must have a magnitude of 1 while the phase must be $\pm 90°$.

This is satisfied when...

$$\frac{L_{perturbed}}{W_{perturbed}} = 1 + \frac{1}{Q_t}$$

With the dimensions fixed, the feed location must be on the diagonal of the rectangular patch to receive RHCP signals. The exact location along that diagonal will determine the impedance of the antenna. In general, the impedance gets reduced from the edge by the factor $\cos^4\left(2\pi\delta/\sqrt{L^2+W^2}\right)$ and goes to zero at the center of the patch. An impedance of 50 ohms requires the feed at approximately 34% of the distance from center to edge. For an in depth consideration of the above derivation, please see [James].

The patch antenna designed and constructed for the research presented in this dissertation is shown below. This antenna has a substrate level that is 0.3125 cm thick with a dielectric constant of 9.2. These particular values were chosen from a limited list of available substrate materials to produce compact size GPS L1 patch antennas [Kim 04].

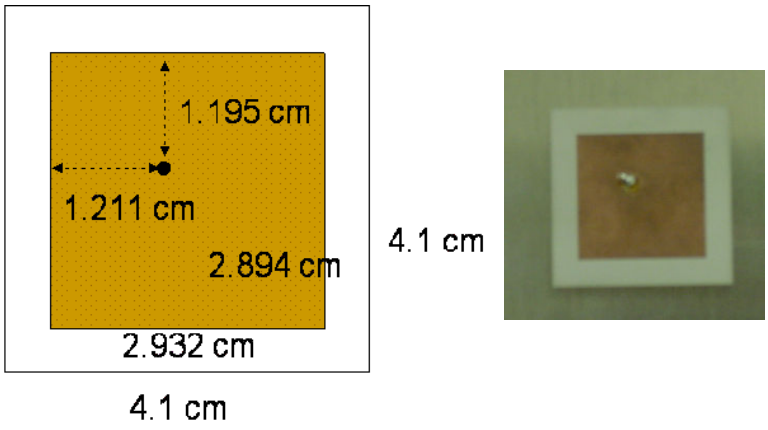

Figure 2-3. Patch Antenna Constructed at Stanford University GPS Laboratory

As can be seen in Figure 2-3 this is a rectangular patch antenna with a single coaxial probe feed located on the diagonal of the rectangular patch. This rectangular patch along with the single diagonal feed provides the capability of receiving RHCP (Right Hand Circularly Polarized) signals. The location of the feed on the diagonal determines the impedance of the antenna (in this case, matched to 50 ohms). The dimension of the rectangle's sides, along with the dielectric constant of the substrate, determines the center frequency of the antenna.

These antennas were constructed using double copper clad dielectric material from the Rogers Corporation. The patch geometry and probe feed location were milled and drilled using a CNC milling machine with a dimensional tolerance of approximately 0.01 mm. Twelve antenna elements were constructed in total to investigate both stand-alone and CRPA array configurations.

All antennas have some variation in received carrier phase versus incident signal direction due to the change in the geometry presented to the wave (incident wave location, antenna structure orientation, etc). In other words, the received carrier phase will change if the antenna is rotated. The rectangular patch shown in Figure 2-3 certainly has this property – its geometry varies with the direction of the incident wave. This will result in a different electric field pattern generated for each incident signal direction, and thus, variations in the received signal amplitude and phase.

Importantly, these variations are functions of frequency, as well as elevation (Θ) and azimuth (ϕ). So, each element (and indeed the entire array) is characterized by an amplitude and phase that varies with frequency, azimuth angle, and elevation angle. This can be expressed as a transfer function shown below. These functions are central to this dissertation and the focus of this chapter.

$$H(\omega,\theta,\phi) = Mag[H(\omega,\theta,\phi)]e^{jPhase[H(\omega,\theta,\phi)]}$$

2.2.2 DATA SOURCES

One of the important goals of this research is to use a software model (also known as simulation) to generate predicted phase response maps for each of the antenna elements in any given CRPA configuration, and to generate a correction by fitting a compensation function to these phase maps. These models can be used to accurately

predict and compensate for the phase response variations seen in patch antennas and CRPAs. Before this can be done confidently, the ability of the simulation tool to accurately predict the actual phase response must be validated. This will be done by comparing scans taken in an anechoic chamber to the phase responses predicted by the software.

The software antenna models use Ansoft's HFSS (High Frequency Structure Simulator) package. It is a full 3D Finite Element Method (FEM) field solver of Maxwell's equations with an error based iterative mesh generation feature which makes creation of structures and geometries very easy. However, a drawback to this code package is the long running times [Swanson]. A full "scan" of a single stand alone patch antenna with about 162 incident signal directions in the visible upper hemisphere of the antenna has simulation times on the order of 2-3 days on a machine with a Pentium IV 3.2 GHz processor with 2 GB of memory. Due to the very long simulation times, function fitting to the phase response maps presented below will be fit to the chamber data. This will demonstrate the ability of simple function fitting in matching and predicting the actual phase response of antenna elements in CRPAs. Anechoic chamber testing was done at the Avionics Engineering Center (AEC) in Ohio University shown in Figure 2-4 [Bartone].

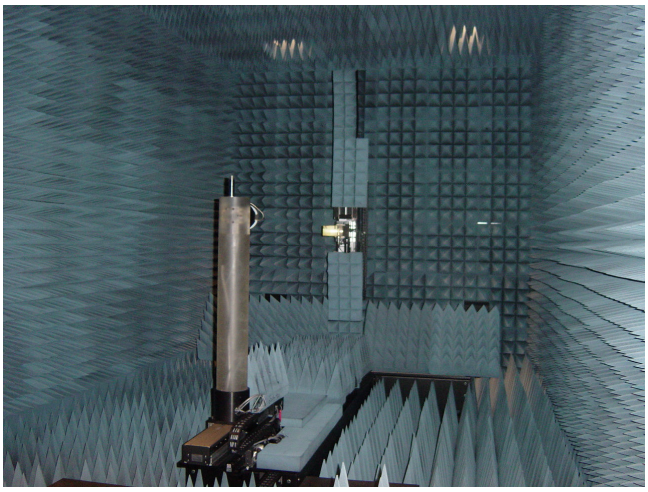

Figure 2-4. Anechoic Chamber at Ohio University's Avionics Engineering Center (AEC)

2.2.3 CHAMBER DATA MEASUREMENT

Twelve patch antennas (shown in Figure 2-3) were constructed in total using a CNC milling machine at Stanford University. In addition, thin inset areas corresponding precisely to the physical exterior dimensions of the antenna, were milled in seven element hexagonal and nine element 3x3 configurations on aluminum ground planes. This allowed free control over the placement and removal of antenna elements as required in precise repeatable locations (Figure 2-5 below).

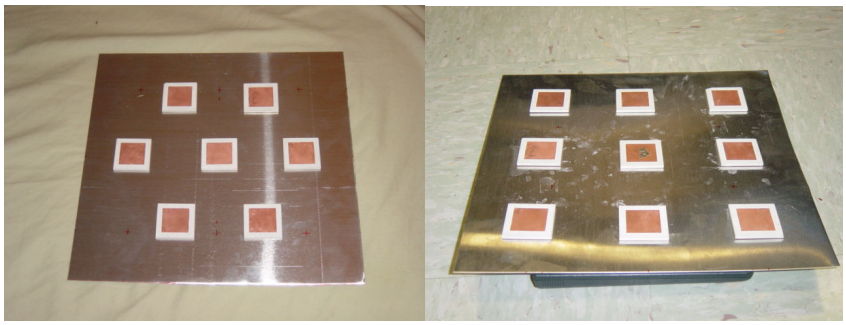

Figure 2-5. Constructed Patch Antennas and Ground Planes in Seven Element Hexagonal and Nine Element 3x3 Array Configurations

The antenna/ground plane combination was fixed securely on the tower arm of the anechoic chamber, and special care was taken to calibrate the set up such that the center of rotation generated by the tower arm corresponded to the feed location on the patch surface of the center antenna element. Data was collected for Right Hand Circularly Polarized (RHCP) signals using Agilent's 8753ES Network Analyzer. The Ohio University AEC's anechoic chamber takes measurements in the near field and performs a near field to far field transformation [Bartone].

2.2.4 Carrier Phase Variation versus Incident Signal Direction

Figure 2-6 below shows the received carrier phase versus incident signal direction for the constructed antenna as taken in the Ohio University anechoic chamber. First, a single stand-alone antenna was placed in the middle of the ground plane and a full scan was taken. The plot is for the upper hemisphere of the antenna. As shown, the

carrier phase varies by approximately 100 degrees. The carrier phase pattern has large carrier phase gradients that correspond to the corners of the antenna.

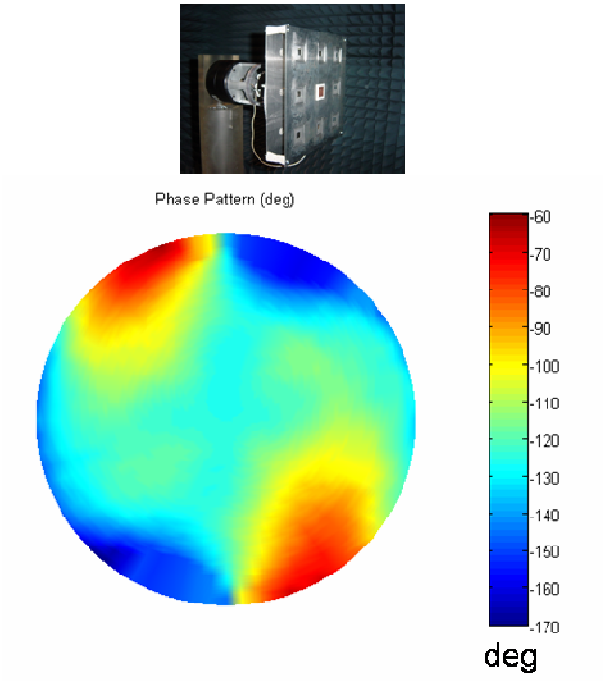

Figure 2-6. Single Stand-Alone Patch Antenna Phase Pattern

Now, keep in mind that we are considering a differential system. Because the signals at reference and user are differenced, one can well imagine these phase variations differencing out if the same antenna is used for both the reference station and the user. In fact, such a cancellation is used in geodesy and precise surveying, where the reference and user antennas can be similarly oriented such that the same phase variations cancel out for all directions. While it is possible to have the two antennas oriented toward a common

reference (typically magnetic North) for surveying and geodesy applications, such an assumption does not hold true for JPALS where the reference and user are both moving platforms that roll, pitch and yaw. So even if the same antenna is used, the variation that is seen above can add a critical component in the error of the differenced carrier phase measurement.

2.2.5 Code Phase Variation versus Incident Signal Direction

In addition to the carrier phase variation presented above, there also exists a variation versus signal direction for the received code phase of the signal, which has a direct influence on the measured pseudorange. The power spectral density of a perfect PRN code sequence is shown below in Figure 2-7. The PRN code sequence that modulates the underlying GPS carrier signal takes the energy of the carrier continuous wave (CW) signal which is concentrated in one frequency and spreads it over the bandwidth shown in Figure 2-7. The peak occurs at the center carrier wave frequency, and the majority of the energy is spread over a 2 MHz bandwidth for the C/A code sequence, and a 20 MHz bandwidth for a P(Y) code sequence.

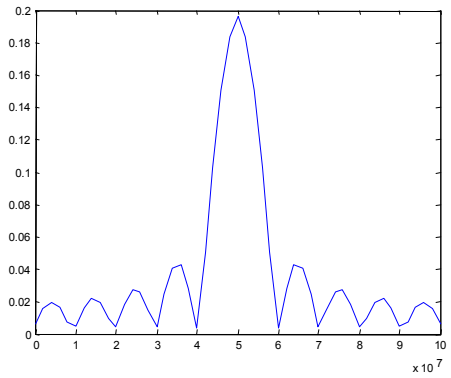

Figure 2-7. Power Spectral Density of the GPS signal (P(Y) coded)

Any biases introduced by the antenna in the frequency content of the signal received will result in a distortion of the PRN code sequence, thus affecting the code phase measurement. Both the amplitude frequency response (antenna gain) and the phase frequency response (group delay) of the patch antenna are considered and their effect on the received code phase of the GPS signal is investigated below.

Figure 2-8 illustrates how this code phase effect is studied. First, the discretized GPS code sequence is converted into the frequency domain via MATLAB's Fast Fourier Transform (FFT) algorithm. Then, the antenna's magnitude and phase frequency responses are multiplied by the frequency content of the GPS code in each corresponding frequency bin. Finally, this altered frequency content is brought back into the time domain via an Inverse Fast Fourier Transform (IFFT). The altered code sequence is then studied in the correlation function to determine the overall effect on the code phase of the GPS signal. Due to limited access to the anechoic chamber, it was impossible to obtain

full scans with enough frequency resolution to capture the required details in the frequency variations to perform the above mentioned analysis. Thus, the results presented in this section are based on HFSS simulation results.

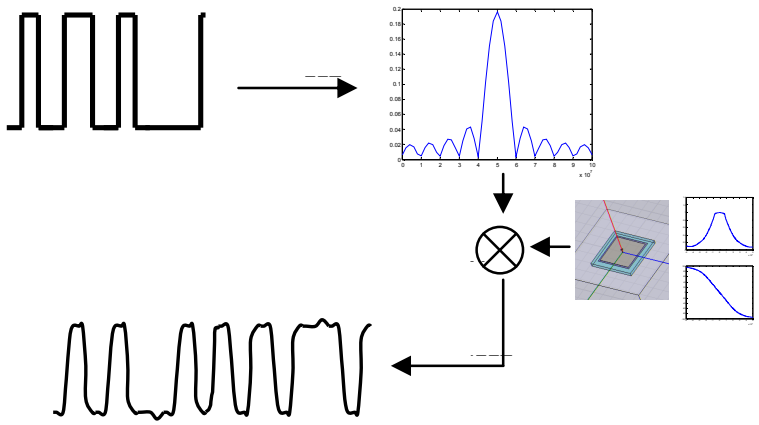

Figure 2-8. Code Phase Investigation of Antenna Frequency Response Effects

Figure 2-9 shown below presents the magnitude and phase response of a stand alone single patch antenna for a variety of incident signal directions. The top two figures show the frequency responses with a sweep in the elevation angle of the incident signal, while the bottom two figures show those for an azimuth sweep in incident signal. The figure shows that the magnitude of the frequency response is more sensitive to the elevation of the incident signal (lower antenna gain at lower elevations), while the azimuth angle of the signal seems to have a more pronounced effect on the phase response.

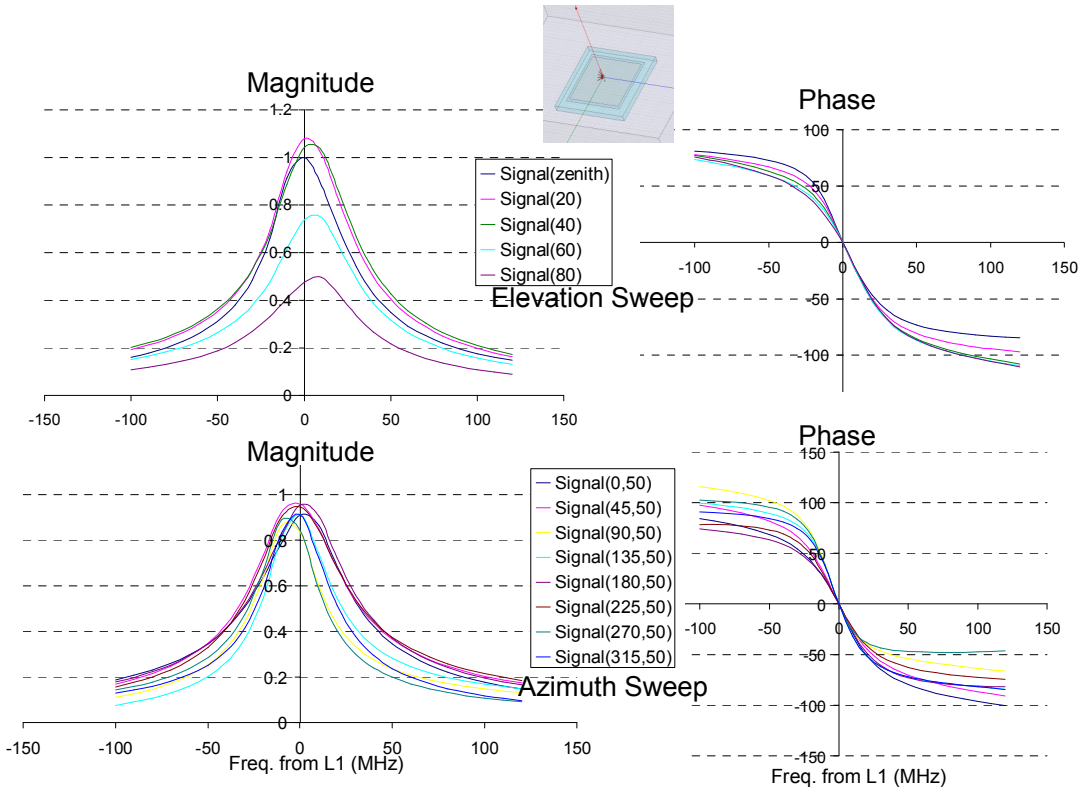

Figure 2-9. Antenna Gain and Phase Response vs. Frequency for Stand Alone Patch

These different frequency responses lead to differing effects on the code phase of the received GPS signal. To help visualize this, Figure 2-10 below shows how a single GPS code chip is affected by the antenna frequency responses presented above. Shown in the figure is a P(Y) code chip with a bandwidth of 20 MHz, which lies mostly in the linear region of the phase response. It shows the filtered P(Y) code chip for different incident signal directions for a single stand-alone antenna. Generally speaking, the magnitude response determines the step size of the chip while the phase response

determines the amount of delay in the chip. The figure shows that certain incident signal directions add more delay in the chip step response. One note of importance is that these incident signal direction effects will be more pronounced when considering P(Y) code chips than for C/A code chips, due to the wider P(Y) bandwidth (20 MHz versus 2 MHz). P(Y) code is used for JPALS because it has better RFI and multipath performance than C/A code. In addition, it is encrypted to mitigate spoofing. However, it does increase the antenna biases considered herein.

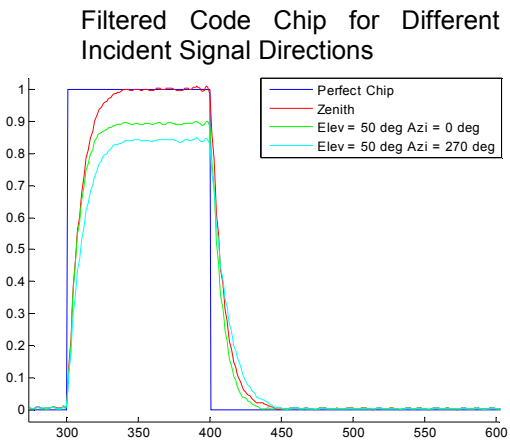

Figure 2-10. Antenna Frequency Response Effect on Single P(Y) Code Chip

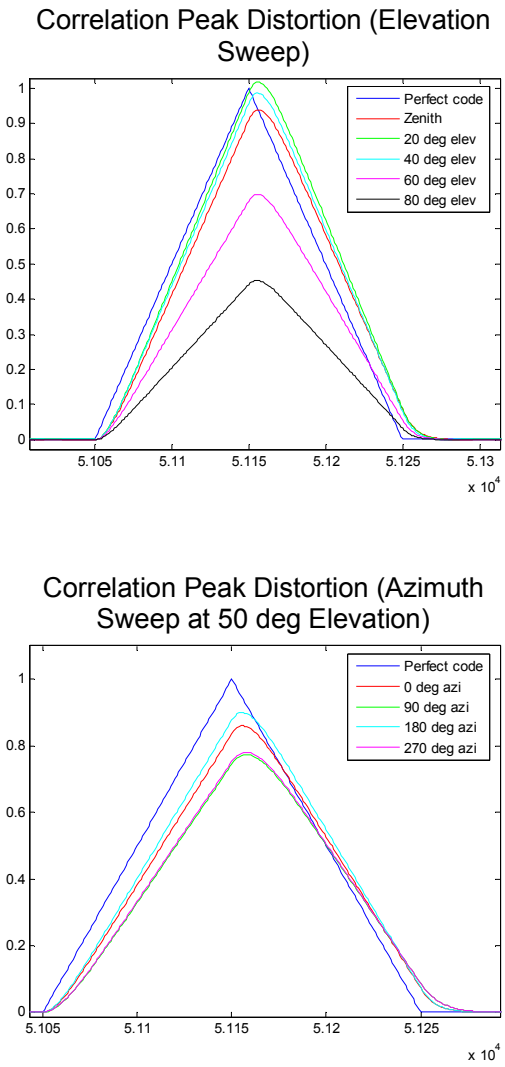

Figure 2-11. Correlation Peak Distortion for Stand Alone Patch

Figure 2-11 illustrates how a sequence of the filtered code chips shown in Figure 2-10 result in a distortion of the correlation peak for each of the cases outlined above. Generally speaking, there is an overall delay effect in each of the cases, in addition to a change in the peak magnitude. Also, there is a slight lean in the correlation peak, i.e.,

the peak is no longer symmetrical. This is a little hard to visualize with the peaks in Figure 2-11, but will become more apparent in the next figure.

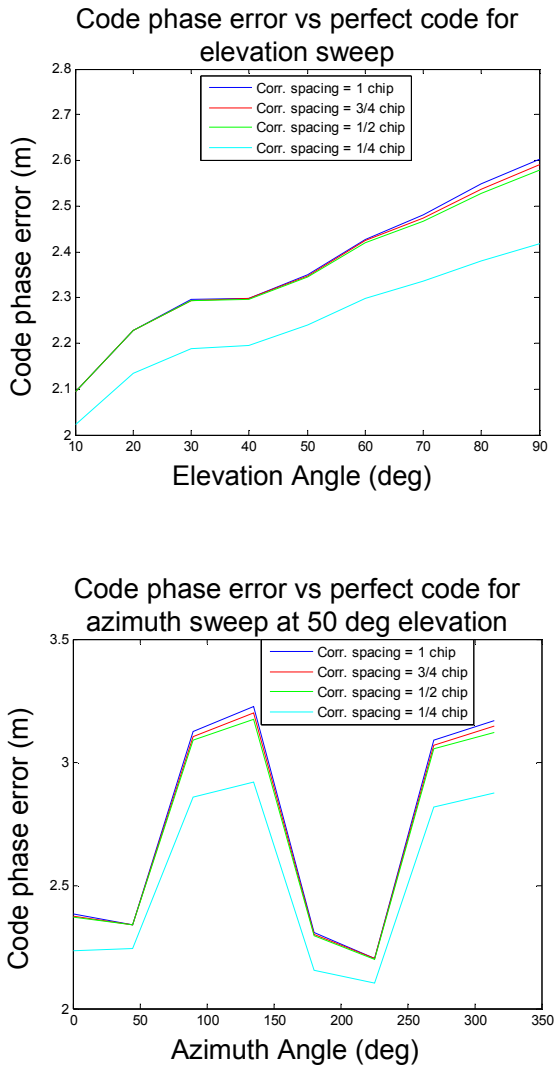

Figure 2-12. Code Phase Error vs. Incident Signal Direction for Stand Alone Patch Antenna

Figure 2-12 shows how the distorted correlation peaks, shown in Figure 2-11, lead to a code phase error. This error is shown for different correlator tracking pair

spacings, which track the location of the peak by equalizing early and late samples. Each of the plots shows the error between the code phase determined from an unfiltered, perfect correlation peak and a correlation peak that has been distorted according to the magnitude and phase frequency responses of the antenna. The code phase error is largest near the zenith of the antenna and slowly decreases as the satellite moves to the horizon. Also notice that the 1-chip, ¾-chip, and ½-chip correlator spacings have nearly identical results, while the ¼-chip correlator spacing leads to a sudden drop in the magnitude of the error. This is due to the lean in the correlation peak that was mentioned above. As the correlator spacing becomes smaller, the pair is tracking closer to the top of the peak which tends toward the perfect correlation peak, more so than the base of the peak. This effect can be seen in both plots shown in Figure 2-11, and this lean in the correlation peak seems to be a general effect of the frequency responses in the antennas under study herein [Kim 05].

The bottom plot in Figure 2-12 shows the errors for an azimuth sweep in incident signal at 50 degrees of elevation. The plot shows that the magnitude of the code phase error has a periodicity as the incident signal sweeps around in azimuth. This rough periodicity is due to the near azimuthal symmetry of the antenna. The plots show a variation in received code phase on the order of about 60 cm in the worst case. This is certainly much larger than a full wavelength. Unless treated, this error will prevent the integer resolution needed for differential carrier phase navigation.

2.2.6 DIFFERENTIAL SYSTEM ERROR

The effects presented above must be viewed in the context of a differential GPS system. As mentioned, Sea based JPALS will be a dual-frequency, carrier phase DGPS system. For a differential system, the important issue is not the absolute code phase error or the absolute carrier phase error, but rather the differential code phase and differential carrier phase errors. Therefore, if both the reference and the user antenna are identical and looking at the same geometry of incident signals, all antenna code and carrier phase errors will be canceled out in the double differencing algorithm, and there will be no need to account for any of the signal biases mentioned above.

However, such is not the case for JPALS. For starters, the reference antenna and the user antenna are most likely not the same antennas, and thus have different magnitude and phase responses. Therefore, some differential code and carrier phase errors will be introduced into the double differenced signal. Even if the reference and user antennas are the same, they will be rotated relative to each other. In the case of Sea based JPALS, the reference antenna on the aircraft carrier superstructure will place all the satellites at a set of elevation and azimuth angles that differ from those on the aircraft. Due to the overall system accuracy requirements, the integers must be resolved with high precision. Thus, the integer ambiguity resolution process starts while the aircraft is far from the reference antenna, and employs averaging to arrive at a first estimate of the integer solution as the user gets closer to the aircraft carrier. This means the process will start well before the plane is on a stabilized landing glide slope, and the satellite constellation geometry seen

at the user and the reference will be different and changing constantly. Thus the signal direction dependent bias characteristics of the antenna will add differential errors due to the different satellite constellation geometries. From Figure 2-12 above, the features of importance are the variations in the code phase biases seen over signal directions, rather than the actual magnitude of the biases.

Looking at the code and carrier phase variations over the incident signal directions, we can see that the single stand alone patch antenna is not adequate for carrier phase differential GPS positioning. Not only that, a stand alone patch is susceptible to RFI and has no innate interference rejection capabilities. In the following chapter, we will investigate a CRPA system and determine code and carrier phase variations for a CRPA array.

CHAPTER 3: SIGNAL BIASES INTRODUCED BY CRPA ANTENNA ARRAY

In the previous chapter, we were introduced to microstrip patch antenna elements, and saw that stand alone patch antennas were not adequate for carrier phase differential GPS applications. In this chapter, we will see that patch antennas behave differently when populated in an array because of mutual coupling between the individual antenna elements. We will also see that the CRPA algorithm plays a role in the determination of code phase and carrier phase variations for the entire CRPA system. Results will show that integer determination requires treatment of the code and carrier phase variations introduced by a CRPA. We will discuss the required calibration in Chapter 4. Chapter 5 will deal with the overall JPALS system error sources and their effect on carrier phase DGPS processing, with the conclusions and future work following in Chapter 6.

3.1 MUTUAL COUPLING IN ANTENNA ARRAYS

When two antennas are close to each other, they exchange energy and this interchange is known as mutual coupling [Balanis]. Mutual coupling effects are rather difficult to predict analytically, particularly for patch antennas, but they must be taken into account for accurate beam/null steering. Otherwise, the gain afforded by beam steering may be degraded, and additional carrier phase biases may be introduced. Mutual coupling depends on the following factors: the receiving characteristic of each antenna element, the relative separation between antennas, the relative orientation of each antenna element, and the feed network driving the array [Stutzman].

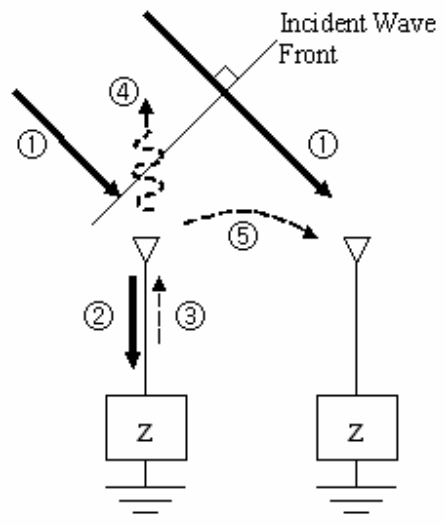

Figure 3-1. Mutual Coupling Path in Receiving Antenna Pair [Stutzman]

To illustrate the mechanism by which mutual coupling occurs, let us look at two passively loaded antenna elements (Figure 3-1). Any incident wave (①) received by the first antenna will impress a current flow in that antenna (②). With an antenna that is well matched to the impedance of the receiver, the current from the antenna (②) will flow unimpeded into the receiver. However, any mismatch in impedance between the antenna and receiver will result in some of the signal being reflected back towards the antenna (③). For GPS antennas, this will almost certainly occur, as it is next to impossible to closely match the impedance of the antenna to the impedance of the connected electronics over the entire bandwidth of the received GPS signal. This reflection results in part of the incident signal being rescattered into space (④), some of which will be directed towards the other antenna (⑤). The signal received at the second antenna will be a vector addition of the scattered signal from the first antenna (⑤) and the original incident wave (①). Similarly, the first antenna will also be subject to mutual coupling effects induced by the scattering wave produced by the second antenna [Stutzman].

For a large array with many antenna elements, fringing effects for those elements near the edge of the array ground plane can be ignored, and the relative shapes of the

individual antenna patterns will be mostly unchanged even with coupling interactions. The only effect will be a scaling up or down in amplitude while the shape is preserved. However, for smaller arrays such as ours, the edge effects become more dominant and mutual coupling will affect the antenna pattern [Visser].

These mutual coupling effects in an array can be understood using standard circuit analysis. Suppose we have an array of N elements. They can be treated as an N port network as follows

$$\begin{aligned} V_1 &= Z_{11}I_1 + Z_{12}I_2 + \cdots + Z_{1N}I_N \\ V_2 &= Z_{21}I_1 + Z_{22}I_2 + \cdots + Z_{2N}I_N \\ &\vdots \\ V_N &= Z_{N1}I_1 + Z_{N2}I_2 + \cdots + Z_{NN}I_N \end{aligned} \qquad \text{Eqn (3-1)}$$

where V_n and I_n are the impressed voltage and current in the n^{th} element, and Z_{nn} is the self-impedance of the n^{th} element. The mutual impedance, Z_{mn}, between elements m and n will be reciprocal (i.e., $Z_{mn} = Z_{nm}$), assuming all elements are identical [Balanis]. This is a straightforward representation of mutual coupling effects. However, the actual impedance terms are rather difficult to obtain. For a transmitting array where one has control over the excitation currents in each channel, each of the self and mutual impedance terms in (6) can

be determined using careful experimental measurements. For this application, frequency dependent antenna impedance characteristics must be known as well to determine the exact effect on the GPS signal, and the experimental measurement of mutual coupling starts to become a daunting task. This becomes even more difficult when considering a receiving antenna array. Even though all antennas are reciprocal, it is more difficult to get independent experimental measurements that isolate each mutual impedance term in the above equation for a receiving case where the excitation source is an incoming radio wave that impinges on all the array elements at once. Thus, mutual coupling effects in receiving arrays are easier studied in terms of the overall impedance in each channel, rather than breaking down into individual self and mutual impedance terms. This is the approach that will be taken in this dissertation, and the mutual coupling on each antenna element will be analyzed according to the impact on the magnitude and phase of the received GPS signal.

3.2 MUTUAL COUPLING EFFECT ON RECEIVED CARRIER PHASE OF PATCH ANTENNA ELEMENTS

Figure 3-2 shows the effects mutual coupling can have on the received phase response of an antenna element. The figure shows phase maps of the center antenna element with a 50 ohm terminated antenna located at the identified positions around the center element at half wavelength baseline. As shown, mutual coupling definitely has an effect on the phase response of the antenna. The magnitude and angular location of this effect is dependent on the relative location of the antenna element inducing the mutual coupling effect. The observed maximum difference in the phase response between a single antenna element and that of an antenna element that is under coupling effects from an adjacent element in any given direction is about 40 degrees. This demonstrates that mutual coupling can introduce phase effects that are dependent on the configuration of the antenna array. With the combined effects of mutual coupling and fringing effects, one can expect each of the antenna elements in any CRPA to have a different phase response map.

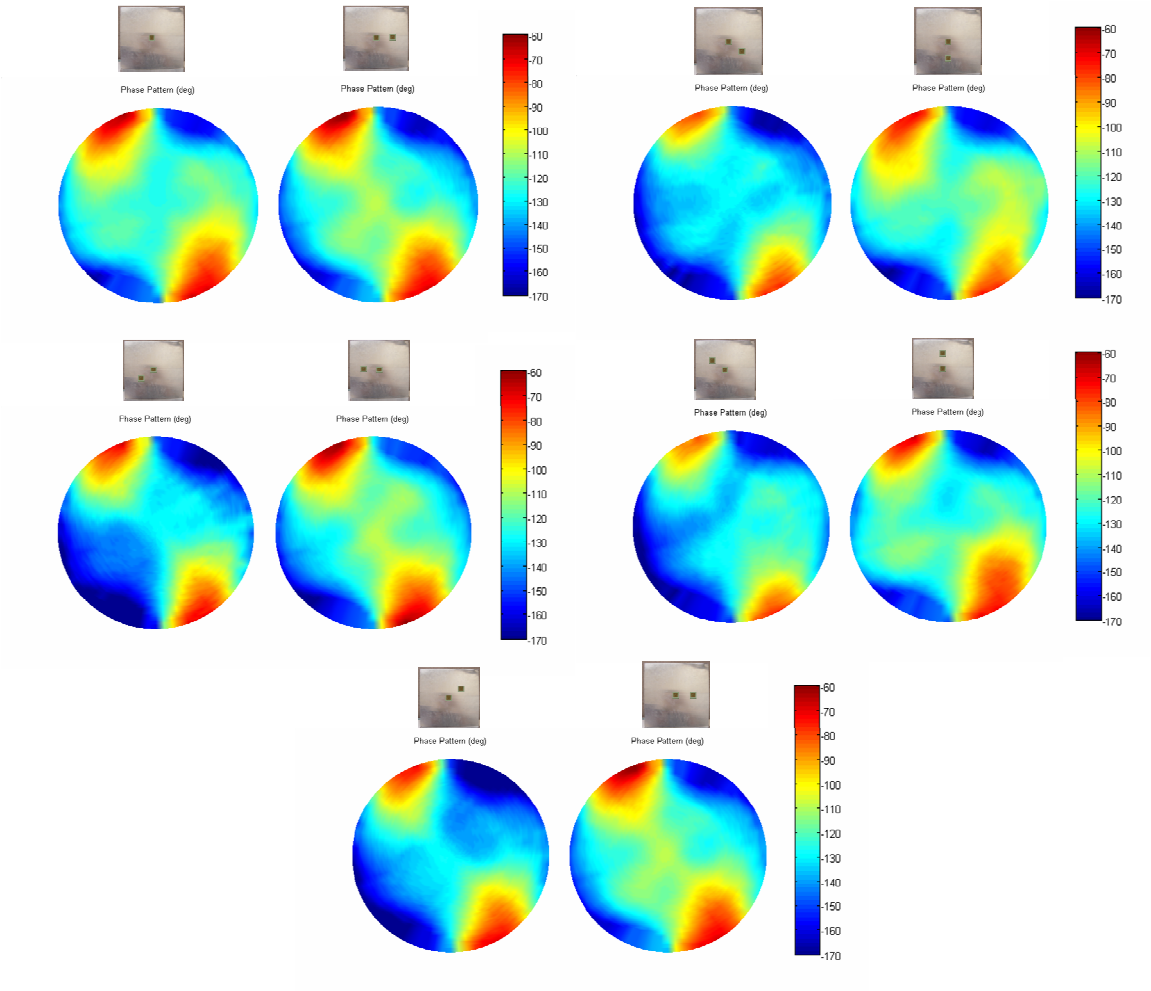

Figure 3-2. Effects of Mutual Coupling on the Phase Response of the Antenna

3.3 MUTUAL COUPLING EFFECT ON RECEIVED CODE PHASE OF PATCH ANTENNA ELEMENTS

Figure 3-3 illustrates the effect that mutual coupling can have on the frequency response of the antennas. The magnitude and phase frequency responses are shown for a signal coming in at zenith for three different cases: single stand-alone antenna; the center element of a hexagonal, half-wavelength baseline, seven-element array; and an edge element in that same seven-element array. This shows that a given antenna element can have rather different frequency response characteristics, depending on the configuration of the adjacent elements which dictate the mutual coupling environment of the antenna element. The magnitude plot on the left has been normalized versus the L1 magnitude value for the stand alone antenna. A very interesting phenomenon that we see in this plot is that mutual coupling effects can actually combine constructively to increase gain for certain elements in an array as compared to a stand alone antenna.

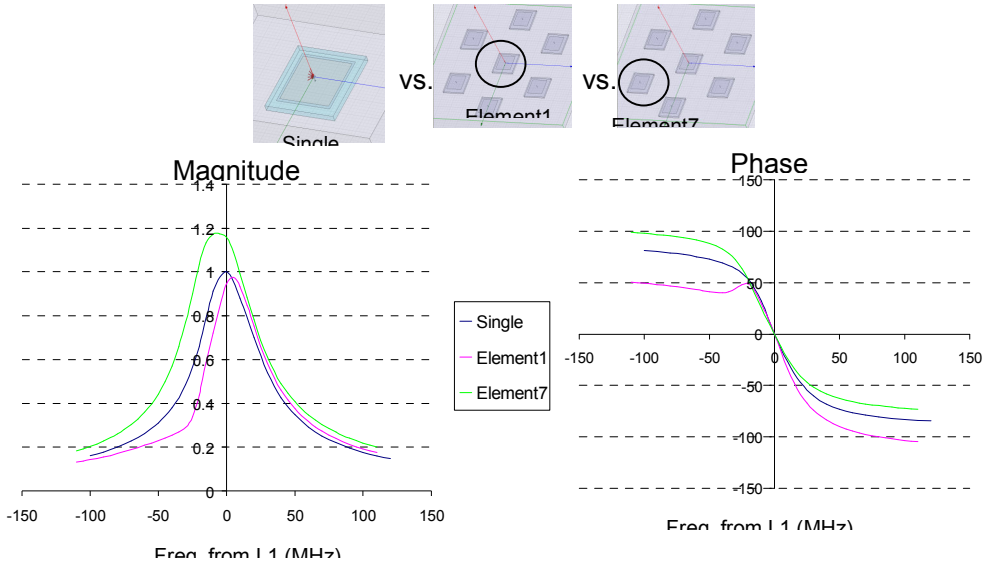

Figure 3-3. Frequency Response Comparison of Single Antenna vs. Different Antenna Elements in a Seven Element CRPA for a Signal from Zenith (HFSS Simulation Data)

These different frequency responses lead to differing effects on the code phase of the received GPS signal. Figure 3-4 shows the effects of the antenna filtering on the P(Y) code chip of the GPS signal. The first figure shows the filtered P(Y) code chip for different incident signal directions for two different elements in an array receiving the same signal. The magnitude response determines the chip amplitude while the phase response determines the amount of delay in the chip. Any asymmetries in the magnitude response about the center L1 frequency will result in an asymmetric distortion of the time response (i.e., effect on leading step is different from effect on trailing step), thus leading to received

code phase variations. The figure shows that certain incident signal directions and certain elements in an array add more delay in the chip step response due to the unique mutual coupling environment seen by these elements. Again, the magnitudes of the responses show that mutual coupling can lead to constructive combination of scattered energy, leading to an increase in gain for certain elements in an array as compared to a stand alone antenna case.

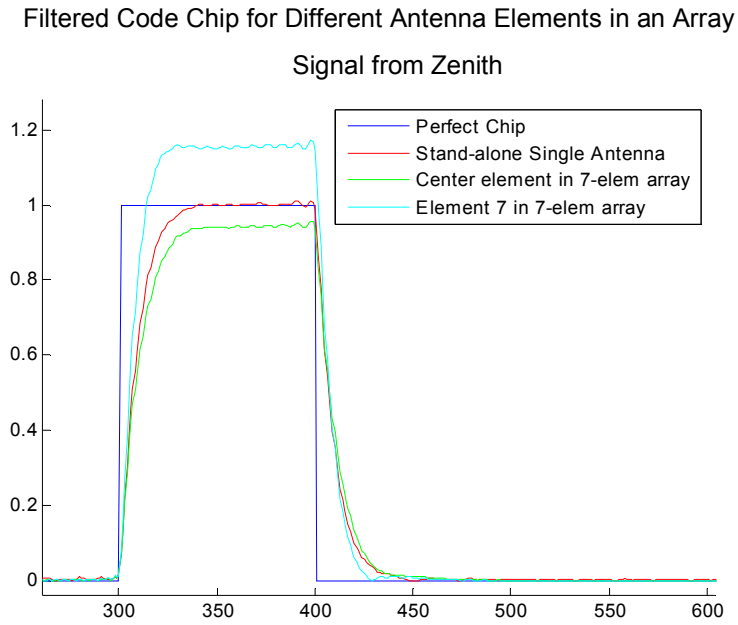

Figure 3-4. Antenna Frequency Response Effect on Code Chip : Seven Element Case

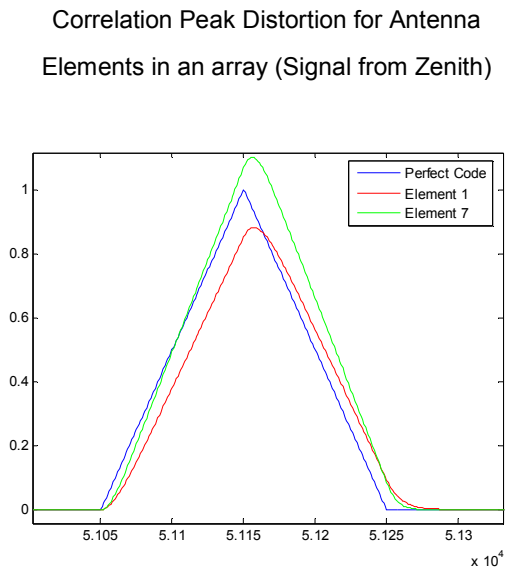

Figure 3-5. Correlation Peak Distortion : Seven Element Case

Figure 3-5 illustrates the distortion that occurs in the correlation peak due to the code distortions seen in Figure 3-4. Keep in mind that these are correlation peaks for a stand alone patch antenna, and for identical antennas populated in two different locations in a hexagonal seven element array. The signal that these three antennas are looking at comes directly from zenith, and the geometry of the problem dictates that all three antennas should receive the same signal (and thus have the same correlation peak). The differences are due to the mutual coupling environment introduced by the adjacent antenna elements in an array. Again, there is an overall delay effect in each of the cases, in addition to a change in the peak magnitude. Also, there is a slight lean in the correlation peak, i.e., the peak is no

longer symmetrical. This is a little hard to visualize in the correlation peak plots, but will become more apparent in the next figure.

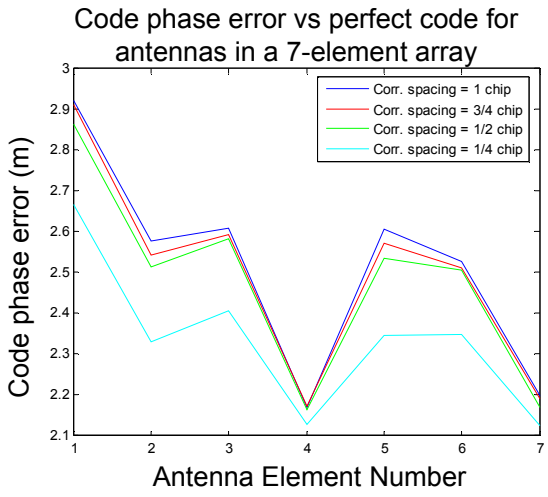

Figure 3-6. Code Phase Errors for Different Correlator Tracking Pair Spacings

Figure 3-6 shows the code phase errors that arise due to the distorted correlation peaks shown in Figure 3-5. This error is shown for different correlator tracking pair spacings. Each of the plots shows the error between the code phase determined from an unfiltered, perfect correlation peak and a correlation peak that has been distorted according to the magnitude and phase frequency responses of the antenna for each of the antenna elements in a hexagonal seven-element array receiving a signal from zenith. Even when all of the antenna elements in an array are receiving the same signal, they all have different

received code phases due to their unique mutual coupling environments. Also note that mutual coupling also affects the amount of lean in the correlation peak. Thus, correlator spacing has an important effect on the impact of the mutual coupling. For example, Antenna Element 4 shows smaller variations in received code phase vs. correlator pair spacing than Antenna Element 1. This tells us that the lean in the correlation peak for Antenna Element 1 is much more pronounced than the lean for Antenna Element 4.

As is clearly demonstrated above, mutual coupling alters the code and carrier phase response of the individual antenna elements populated in an array. Now, let us consider the entire CRPA system and the output signal of the processed CRPA signal. In order to do that, we need to choose a CRPA algorithm to work with.

3.4 CRPA ALGORITHM

Phased array beam-forming is achieved by shifting the phases of each channel signal to combine in-phase, thus creating a more powerful signal [Stutzman]. Figure 3-7 below illustrates this concept in a simple 2D drawing.

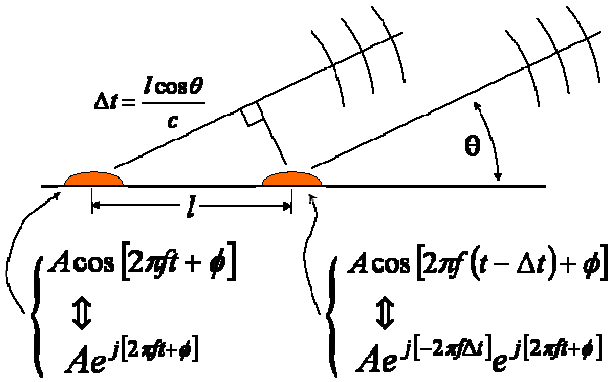

Figure 3-7. Phased Array Beam Forming [De Lorenzo 04]

The received signal in each antenna element can be characterized as a sequence of complex numbers as shown in the representation in Figure 3-7. The real part is the in-phase sample (the I sample) and the imaginary part is the quadrature sample (the Q sample). It is these I/Q samples that are phase shifted by the complex weights determined by the CRPA algorithm. There are many algorithms for determining the required phase shift in each channel. This weighting can be done deterministically by leveraging the knowledge of the geometry of the problem (incident signal direction, and the orientation and baseline of the array), or it can be done adaptively (maximizing signal-to-noise ratio of the GPS signal, minimizing the power of total received signal, driving the weights with reference signal,

etc.) [Widrow],[Manolakis],[Monzingo],[Godara],[Allen],[Visser]. For a typical beam steering algorithm, it can be seen from the element signals shown in Figure 3-7 that when the phase shifting is done precisely, and the "beam" is formed directly at the incident signal, the output signal of the CRPA will be an exact in-phase combination of each channel and will not have any phase biases. For null-steering algorithms, the focus is on the specific placement of nulls in the antenna gain pattern in the direction of interference sources, and the carrier phase integrity of the output signal is compromised.

However, for deterministic beam-forming (DBF), the required phase shifts are calculated based on the geometry of the problem (line of sight vector to satellite, orientation of array, baselines of array elements). This phase shift solution for each element will always be a symmetrical solution, i.e., the required phase shift for Element 2 will be equal in magnitude but just opposite in direction to the required phase shift for Element 5. These pairings will hold true for Elements 3 and 6, and Elements 4 and 7 as well. Please see Figure 3-8 below.

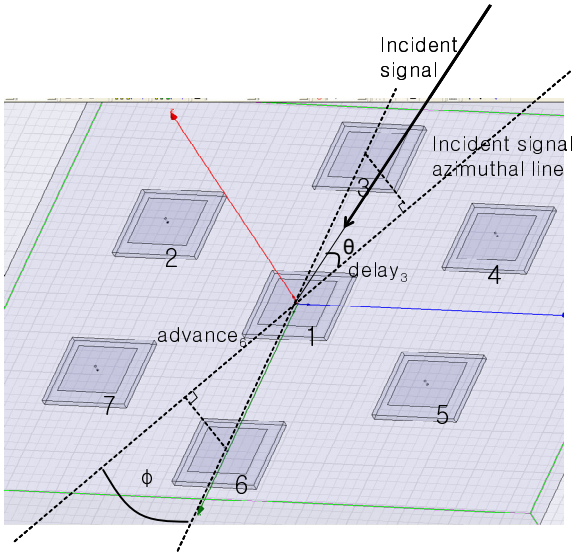

Figure 3-8. Seven Element Hexagonal Array Element Numbering Scheme.

Based purely on the geometry of the above problem, it is readily apparent that the amount of phase delay required to bring the Element 3 signal in phase with Element 1, and the amount of phase advance required to bring the Element 6 signal in phase with Element 1 are identical. Errors in the knowledge of the line of sight to the satellite or the orientation of the array do attenuate the received signal. However, they do not yield carrier phase biases in the output signal. This is because even with errors in beam pointing direction, the required geometry based phase shifts are symmetric. Thus, any unwanted out of phase component added to the Element 1 signal will simply be canceled out by its corresponding counterpart signal that carries the exact opposite out of phase component. The only effect is

that the elements are no longer combining exactly in phase resulting in a smaller gain versus the perfect beam-formed signal. This ideal property may not hold for adaptive algorithms unless there is a geometric symmetry constraint on the weights [Kim 05].

In general, an adaptive algorithm without constraints is unsuitable for use in a carrier phase differential GPS system, like Sea based JPALS, where carrier phase integrity is essential to meeting overall system accuracy, integrity, availability, and continuity requirements. Figure 3-9 below will help illustrate this point.

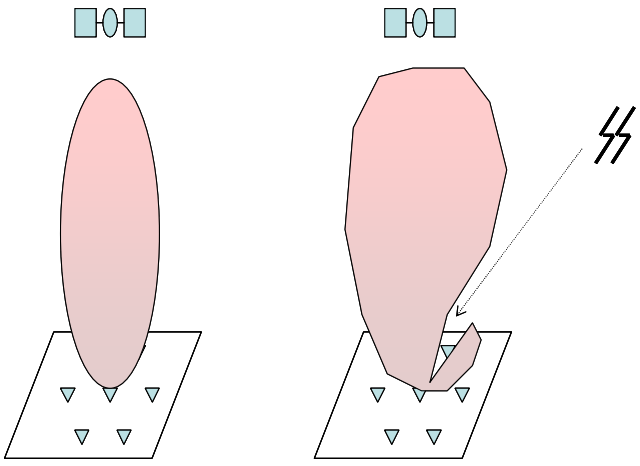

Figure 3-9. Deterministic beam forming vs. adaptive processing

The image on the left in Figure 3-9 represents a nominal state case where there are no interference or multipath sources. Both the deterministic and adaptive methods will ideally have the same result: the boresight of the beam pointed directly at the satellite. However, interference is present in the right hand figure. Any type of adaptive algorithm (whether it is trying to maximize the GPS signal to noise ratio or minimize the overall received power) will shift the weights such that the boresight of the beam is no longer pointed straight at the satellite, and a null is placed in the direction of the interference source. Even though the interference may be rejected, the output of the CRPA will now have a phase bias associated with the weights that were shifted to create the null. A deterministic system will keep the boresight of the beam pointed towards the satellite and not introduce any phase biases, even if the received GPS signal-to-noise ratio (SNR) may be a little weaker than an adaptive array due to the interference. It will be better to perhaps give up a little bit of RFI protection for a guarantee of phase integrity. The obvious problem occurs when the interference source is too close to the incident signal direction, but such a case is a difficult scenario to handle even for an adaptive algorithm. For these reasons, the remainder of this research is based on a parallel "channel" deterministic beam-forming scheme to point the boresight of the beam towards a given satellite in each "channel."

In order to minimize phase biases for such a scheme, there are a few requirements. The geometry of the problem must be well known (even though the algorithm itself will not introduce carrier phase biases as discussed above, it is important to minimize the errors introduced by the antenna element frequency responses and mutual coupling). Also, the code and carrier phase center movement (versus incident signal direction) of each antenna element must be modeled accurately and compensated for. Even though this method has some additional requirements as compared to adaptive processing, the greater confidence in the integrity of the code and carrier phase of the CRPA output signal makes it worthwhile.

It is worth noting that even if we did investigate an adaptive algorithm, the code and carrier phase center variations induced by the antenna hardware must be modeled and compensated for in order to obtain as close to an unbiased signal as possible. The preference for a beam forming solution over an adaptive solution comes from the signal bias characteristics of the algorithms themselves. Beam forming does not introduce additional biases, whereas the same cannot be said for adaptive algorithms.

3.5 EFFECT ON COMBINED CRPA OUTPUT SIGNAL

Taking all of the individual antenna element code and carrier phase effects outlined so far in previous chapters, and implementing a deterministic beam-forming algorithm mentioned above, the effect on the code and carrier phase of the CRPA output signal can now be studied. Figure 3-10 illustrates how this is investigated in simulation.

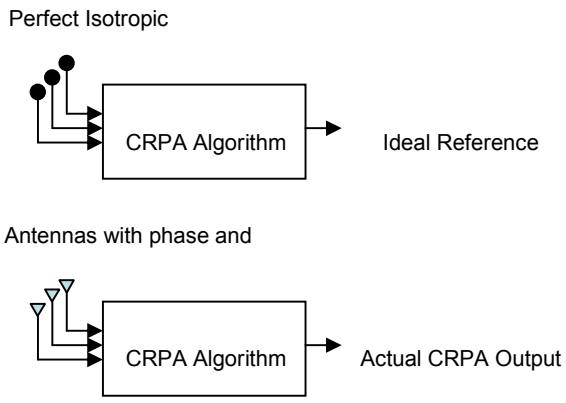

Figure 3-10. Flowchart for CRPA signal simulation

For a given satellite, the signal is received by a hexagonal, seven-element, half-wavelength baseline antenna array composed of perfectly isotropic receiving elements. These signals are I/Q sampled and multiplied by complex weights to form an exact beam towards the satellite, and the output of that algorithm is taken as a “truth” reference. Then the process is repeated with antenna elements which include all of the carrier phase and

code phase biases outlined above. Again, after the beam-forming algorithm, this CRPA output signal is compared to the isotropic array "truth" signal to determine the overall bias in code and carrier phase of the CRPA.

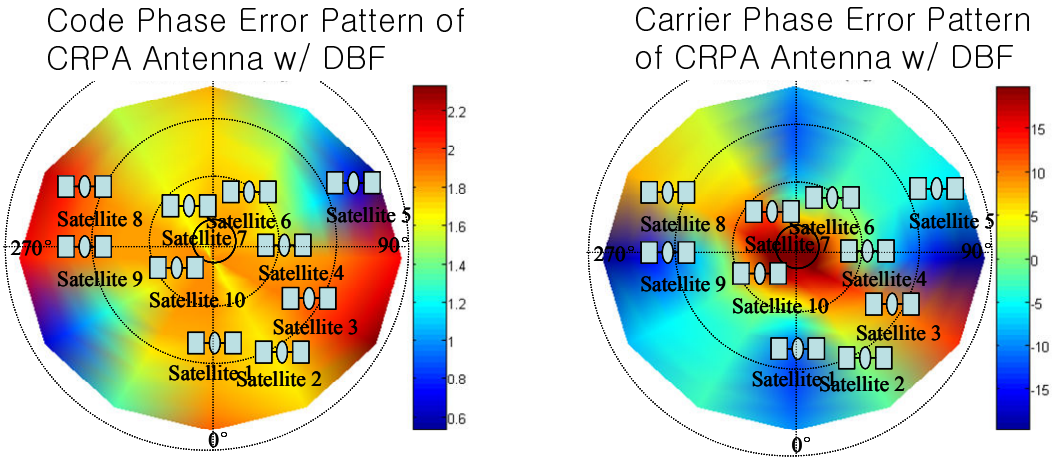

Figure 3-11. Sample constellation

Figure 3-11 shows a sample constellation that we will use to investigate CRPAs and their adequacy for use in a carrier phase differential GPS system. The constellation was chosen carefully to incorporate worst case differential error pairings between satellites. Figure 3-11 shows the sample constellation overlaid on top of the CRPA system code and carrier phase error deviations from the isotropic geometry only solution. Upon inspection, it is apparent that the constellation was chosen carefully to incorporate worst case differential

error pairings in both cases: Satellites 5 and 8 for code phase error, and Satellites 9 and 10 for carrier phase error. The line-of-sight directions and the code and carrier phase errors for each satellite are presented in Table 3-1 below.

SV	Azimuth (deg)	Elevation (deg)	Code Phase Error	Code Phase Variation vs mean	Carrier Phase Error	Carrier Phase Variation vs mean
1	0	40	2.463	-0.138	-12.7	12.5
2	30	30	2.227	0.099	-3.4	3.2
3	60	40	1.955	0.371	-4.7	4.5
4	90	50	2.506	-0.181	-7.2	7.0
5	120	20	2.743	-0.418	7.0	-7.2
6	150	60	2.326	-0.001	10.5	-10.7
7	210	70	2.491	-0.166	6.5	-6.7
8	240	20	1.381	0.945	-5.0	4.8
9	270	30	2.621	-0.296	-16.4	16.2
10	300	80	2.542	-0.217	23.7	-23.9
		Max Diff.	**1.36**		**40.1**	

Table 3-1. CRPA Hardware Biases for Sample Constellation (Code Phase Error at ½ Chip Correlator Spacing)

While these numbers look rather disconcerting, keep in mind that these are the absolute bias values. As mentioned before, we are concerned with differential bias residuals in the double differenced signals. To get a feel for how bad the differential bias residuals could be, the last row of Table 3-1 lists the largest difference pair in the constellation simulated above. This shows code phase maximum difference of 1.36 meters and carrier phase maximum difference of 40.1 degrees. Without correction, the code phase difference

certainly prevents reliable integer determination. The carrier phase difference would also threaten the integrity of the integer resolution process [McGraw].

The above results show that the magnitude of code and carrier phase variations seen for a CRPA array are on similar orders as those for a stand alone antenna. The carrier phase response is slightly better than the stand alone case, as the variation in carrier phase of the CRPA output signal is based solely on the residual differences in the individual element carrier phase patterns. This amount of variation was attributed to mutual coupling with the phase response plots shown in Figure 3-2. This is great since we were able to buy some interference rejection capabilities from the CRPA while not making the code and carrier phase variation problem any worse. However, a problem remains in that we are not close to being adequate to resolve integer ambiguities. An additional calibration step must be taken to try to undo the antenna frequency response effects which distort the received signal and add biases to it. Chapter 4 proposes a calibration that will enable performance that approximates the geometry only situation, i.e., the received signal will be representative of the geometric center of the receiving antennas.

CHAPTER 4: SIGNAL BIAS MITIGATION FOR CRPAS

As discussed in the previous chapter, deterministic beam formed CRPAs provide a level of protection against interference sources, but their code and carrier phase variations make them unsuitable for integer ambiguity resolution. There are numerous methods one can employ to compensate for and remove these signal bias variations. This chapter introduces two different mitigation schemes for modeling and undoing these biases that bookend the realm of possible mitigation schemes. Only with a successful mitigation scheme can we use CRPAs to enjoy RFI benefits and still solve for integer ambiguity.

4.1 CODE AND CARRIER PHASE VARIATION COMPENSATION SCHEMES

Two separate methods for compensating code and carrier phase variations of CRPAs are presented below. The first is for a deterministic beam-formed CRPA which will

allow the use of polynomial function fitting to model variation effects. This is shown in Figure 4-1 below. We will call this the *CRPA system polynomial model*.

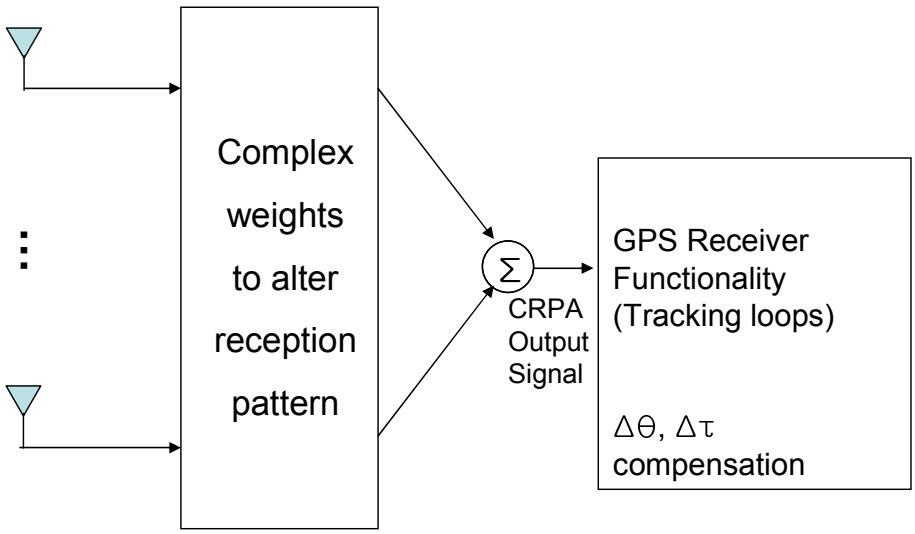

Figure 4-1. CRPA System Polynomial Model Fitting Scheme

In this scheme, the mitigation of the bias effects occurs at the CRPA output, after the signal has gone through complex weighting in each channel and combined according to the CRPA algorithm chosen. The code and carrier phase bias at the output will be a function of the azimuth and elevation of the satellite signal received (antenna bias effects for each element), as well as the specific weights used for reception pattern alteration. We can take one extra step to greatly simplify this scheme. By using a deterministic beam-forming algorithm, the complex weights used in each channel are themselves just a function

of azimuth and elevation of the satellite signal received. Thus, we are left with code and carrier phase biases at the CRPA output that are solely a function of the incident signal direction. Basically, the entire CRPA system can be treated like a single antenna, and a code and carrier phase map can be generated using the individual antenna element characteristics in combination with the beam-forming algorithm. Finally, a polynomial function fitting can be performed to create a model of the code and carrier phase bias variations as a function of azimuth and elevation. The data source for the individual antenna characteristics can come from either a validated simulation or direct chamber measurements.

The great benefit of this scheme is that it is simple compared to the algorithm described later. The information needed to implement this model is just the coefficients of the polynomial terms in azimuth and elevation. The implementation itself is a simple procedure that can be contained in existing hardware. The CRPA output signal is fed into the GPS receiver for tracking. The correction based on the model prediction can be just a slight adjustment to the tracked signal code and carrier phases within the GPS receiver. Additionally, the deterministic beam-forming algorithm does not add biases due to the

algorithm. The only possible drawback is that we are constrained to the beam-former algorithm, which does not reject RFI as well as some other adaptive algorithms. Thus, we give up some RFI protection for signal integrity, something that cannot be guaranteed when using current adaptive algorithms.

The second compensation method presented here is the *channel equalization* method in which each individual antenna element characteristics are compensated for before the CRPA algorithm is applied (Figure 4-2).

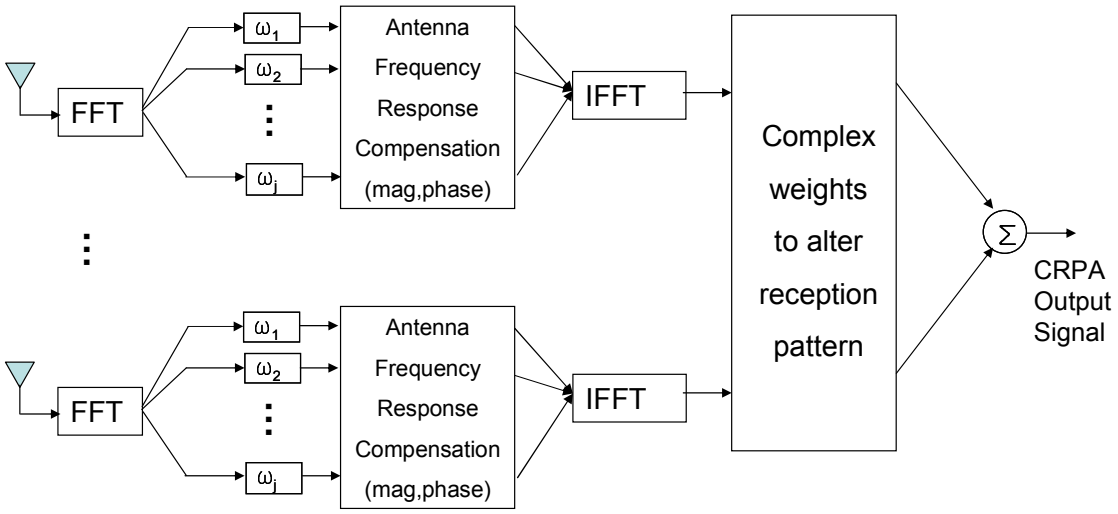

Figure 4-2. Channel Equalization Scheme

In this mitigation scheme, each individual antenna element is compensated before each signal is weighted and combined to form the CRPA output signal. Basically, the

antenna frequency responses covered in Chapter 3 for antenna array elements will be "undone" in each channel, including all mutual coupling effects. Both code and carrier phase biases will be removed as a result of this frequency response compensation. By performing this compensation before any complex weighting, each channel arrives at the isotropic geometry only solution. Each channel signal can then be weighted and combined with the knowledge that all antenna biases have been removed.

A current hotbed of research involves an adaptive CRPA algorithm that provides the RFI benefits of an adaptive algorithm, while at the same time minimizing impact on signal integrity (biases added by the algorithm) [De Lorenzo 06], and channel equalization could make a great match with such an algorithm for Sea based JPALS. It must be noted that no CRPA algorithm will be able to automatically compensate for antenna hardware effects without prior knowledge of the antenna biases, and a compensation scheme for these effects will always be required.

In terms of implementation and hardware requirements, the channel equalization compensation scheme is the most complex. First, the number of frequency bins must be adequate for accurate compensation. The information that is stored for this compensation

must include the magnitude and phase data in the requisite frequency bins with a dense enough grid of azimuth and elevation signal direction points to allow extrapolation of in-between points for each antenna element. This is significantly more information than was required by the CRPA system polynomial fit model. However, it is probably not prohibitive given today's computing and memory standards. In addition, our equalizer architecture also requires FFT and IFFT modules in each channel of the CRPA antenna electronics. However, if a Spectral Frequency Adaptive Processing (SFAP) algorithm is chosen for the weighting algorithm, then the FFT and IFFT modules are already needed, and the antenna effect channel equalization can occur in conjunction with the weight adaptation in each frequency bin. Once again, it must be noted that current adaptive algorithms have no constraints on the weights, nor do they have any "truth" reference to which the adaptive process can be driven. It is an unfortunate byproduct that adaptive algorithms will introduce additional signal biases at the CRPA output as a byproduct of the algorithm itself unless appropriate constraints are added.

4.2 CRPA SYSTEM POLYNOMIAL FIT MODEL

First, we will investigate polynomial function fitting in general and its ability to generate accurate models of patch antenna response characteristics.

4.2.1 POLYNOMIAL FUNCTION FITTING

A multivariate least squares function fitting will be performed on a phase variation scan of the constructed patch antenna from the Ohio University anechoic chamber to determine how well simple polynomial base functions can model actual phase effects seen in CRPA elements. The model will be a function of the azimuth and elevation of the incident signal direction, and only the visible upper hemisphere of the antenna response will be fit. The polynomial base function will include all values of azimuth and elevation, and the coefficients of each term will be solved for via a least squares solution to all of the available data points in the chamber data. Figure 4-3 is a fourth order polynomial fit of the single antenna phase response. The plot on the left is the phase response as scanned from the chamber for our stand alone patch antenna, and the plot on the right is the fourth order polynomial fit to this chamber data. The MATLAB plot of the chamber data on the left is in

itself a linear extrapolation between data points. However, the chamber scan data is dense enough (1.2 deg increments) that the plots with the colors filled in is representative of the actual data (linear extrapolation between data points is acceptable due to the close proximity of the grid points). The polynomial fit does a very good job of capturing all of the dominant features of the actual phase pattern. The maximum error between the chamber data and the generated polynomial model is 27.6 degrees, and the standard deviation of all errors is 4.6 degrees.

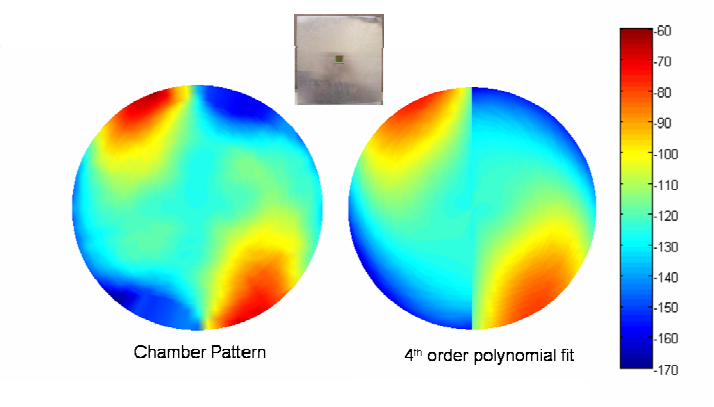

Figure 4-3**.** Polynomial Function Fitting of Single Antenna Phase Response

Figure 4-4 shows a similar function fitting as Figure 4-3, except this time the model is fit to a phase pattern that is asymmetrical due to the mutual coupling effects induced by the 50 ohm terminated antenna element which is added to the upper left of the

data collecting patch. The phase pattern seen from actual scan data (plotted on the left) shows that most of the phase effects induced by mutual coupling manifest in the general direction of the added antenna element. Again, the fourth order polynomial fit does very well in capturing the overall pattern of this asymmetric phase response. However, the errors between the chamber data and the generated model are slightly larger than before. Maximum error is 30.5 degrees and the standard deviation of all errors is 4.9 degrees. The increased errors are due to the more intricate asymmetric pattern to which the polynomial function is fitting. These errors can be reduced by increasing the order of the polynomial model.

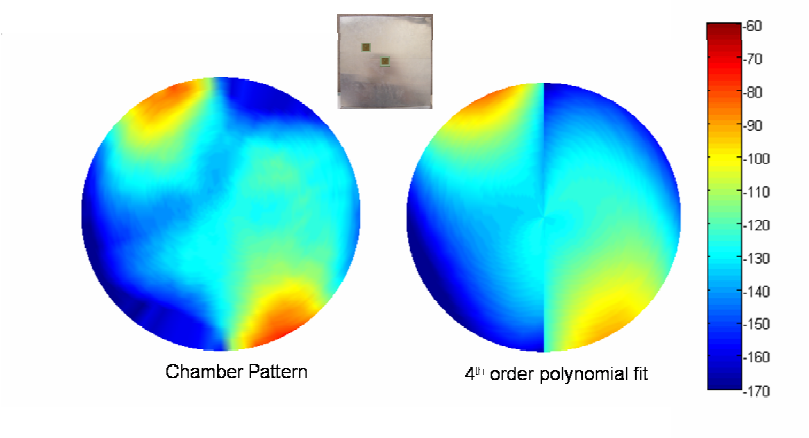

Figure 4-4**.** Polynomial Function Fitting of Mutually Coupled Phase Response

Figure 4-5 demonstrates the benefit achieved through an increase in the order of the polynomial base function of the model. The plots shown here are the phase error maps, i.e., the difference between the scan data and the models generated according to increasing order of polynomials. Using these plots, problem regions where the model deviates from the actual response can be identified. The top left plot is the phase error map for a fourth order fit. The top right plot shows the errors for a fifth order polynomial fit and the bottom plot shows the errors for a sixth order polynomial fit. As the model complexity increases, the problem regions with large errors are significantly reduced.

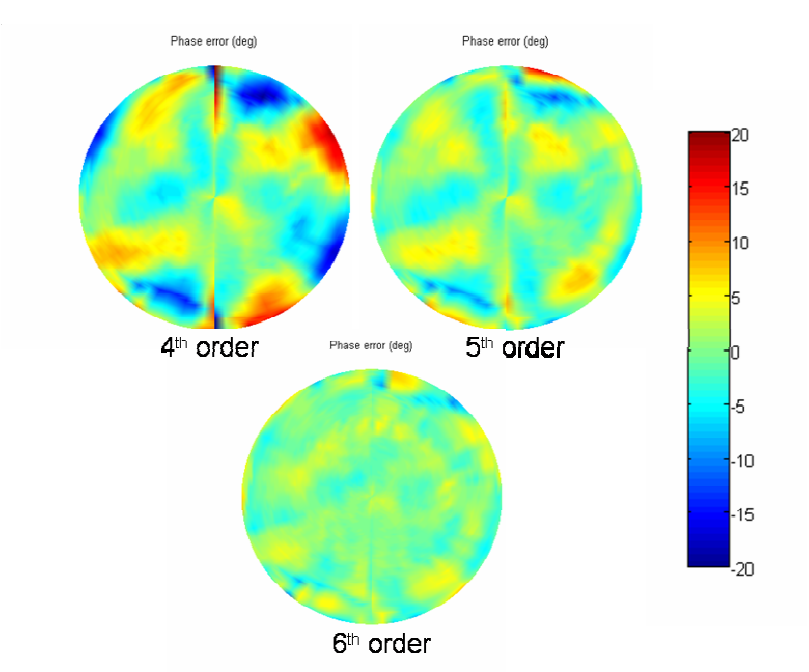

Figure 4-5. Phase Error Maps for Polynomial Function Fits

Table 4-1 shows the benefit obtained in the error statistics by increasing the model complexity. By increasing the complexity to a sixth order polynomial fit, the maximum error between the chamber data and the generated model can be reduced to 10.6 degrees, and the standard deviation of the errors is brought down to 1.8 degrees. The sixth order model does require 49 coefficients as opposed to just 25 for a fourth order model, but these are entirely manageable by today's memory standards.

	4th order	**5th order**	**6th order**
Max (error)	30.5°	16.5°	10.6°
σ(error)	4.9°	3.0°	1.8°
# of coefficients	25	36	49

Table 4-1. Error Statistics for Polynomial Function Fitting

4.2.2. POLYNOMIAL MODELS APPLIED TO DETERMINISTIC BEAM FORMED CRPA SYSTEM

The previous section showed the capability of a simple least squares polynomial function fitting in modeling antenna characteristics of a patch antenna. We saw that this method is capable of capturing fine details introduced by mutual coupling. We can now proceed and use the polynomial function fit to model the code and carrier phase variation of a deterministically beam-formed CRPA output signal. The left plot in Figure 4-6 shows the carrier phase error versus isotropic geometry only solution (signal received at geometric center of array) that was presented in Section 3.5. The right plot is the carrier phase error predicted by a sixth order polynomial model fit to the data shown on the left plot. The bottom plot shows the residual phase error map, or the difference between the left and right plots. As most residuals are contained within ± 4 degrees, polynomial function fitting is quite successful in capturing carrier phase CRPA output variations.

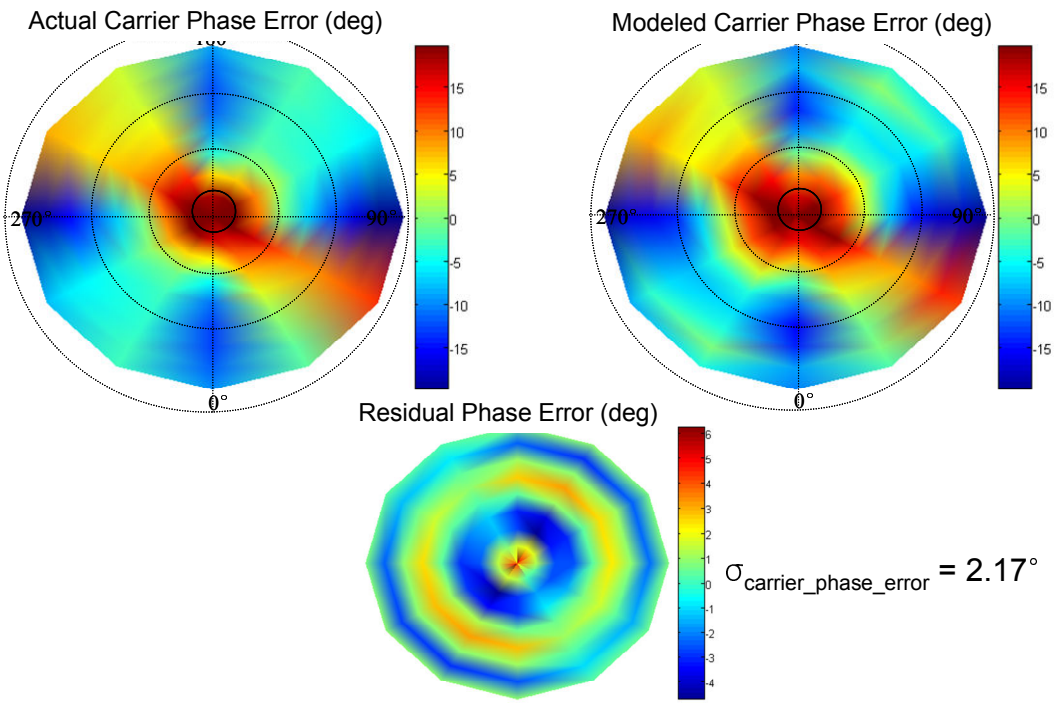

Figure 4-6. Carrier Phase Sixth Order Polynomial Modeling of a Deterministically Beam-Formed CRPA Output Signal

Figure 4-7 shows a similar modeling on the code phase error of a deterministically beam-formed CRPA output signal using the designed patch antennas. Again, the sixth order model captures the code phase variations, with post-compensated code phase error residuals contained within ± 0.015 m.

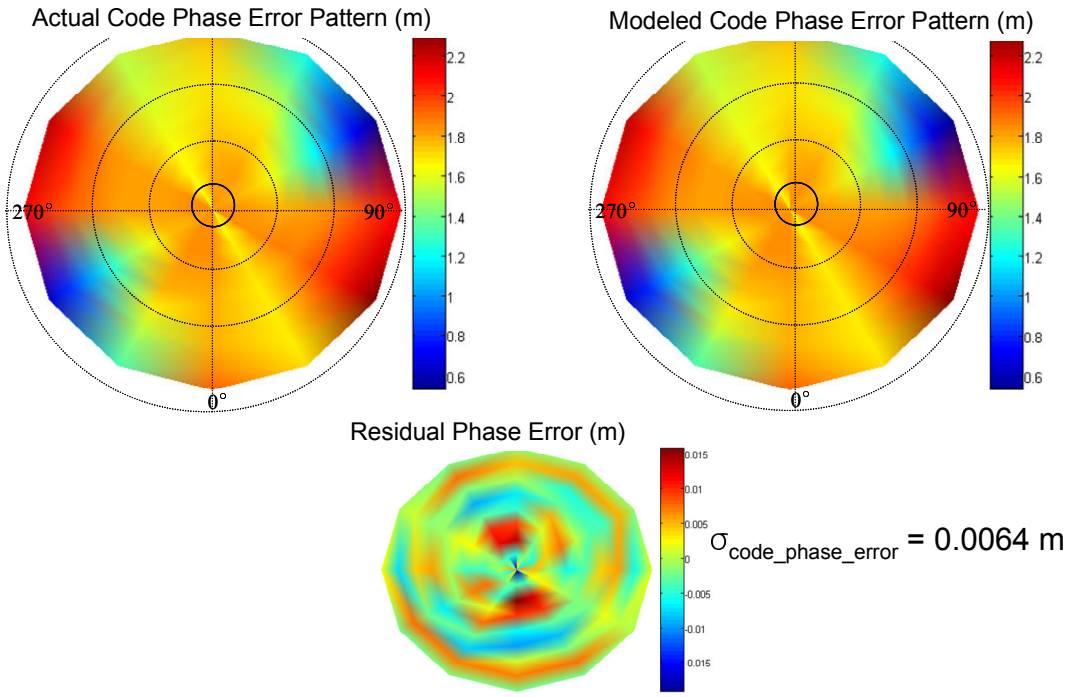

Figure 4-7. Code Phase Sixth Order Polynomial Modeling of a Deterministically Beam-Formed CRPA Output Signal for 1/2 Chip Correlator Spacing

Let us go back to the sample constellation introduced in Section 3.5, and again consider the differential error. Prior to compensation, the largest differential error in code phase in this constellation was 1.36 meters, a level that was completely inadequate for integer ambiguity resolution. However, with the polynomial model fitting, we have reduced that largest differential error to 0.02 meters. We can see a similar benefit for the carrier phase. What was previously a largest differential error of 40.1 degrees drops to 5.0 degrees after the polynomial compensation.

4.3 CHANNEL EQUALIZATION

Channel equalization undoes the frequency response effects of the antenna in each CRPA channel before the signals are processed and combined to form the CRPA output signal. An important consideration is the number of frequency bins that are required to accurately compensate for the antenna frequency response. Compensation in each frequency bin will be based on the actual antenna magnitude and phase response values at the center frequency of each bin. Too few bins and we will not have enough frequency resolution to capture and compensate for the details of the response. Too many frequency bins add unnecessary computing burden without adding any further benefits.

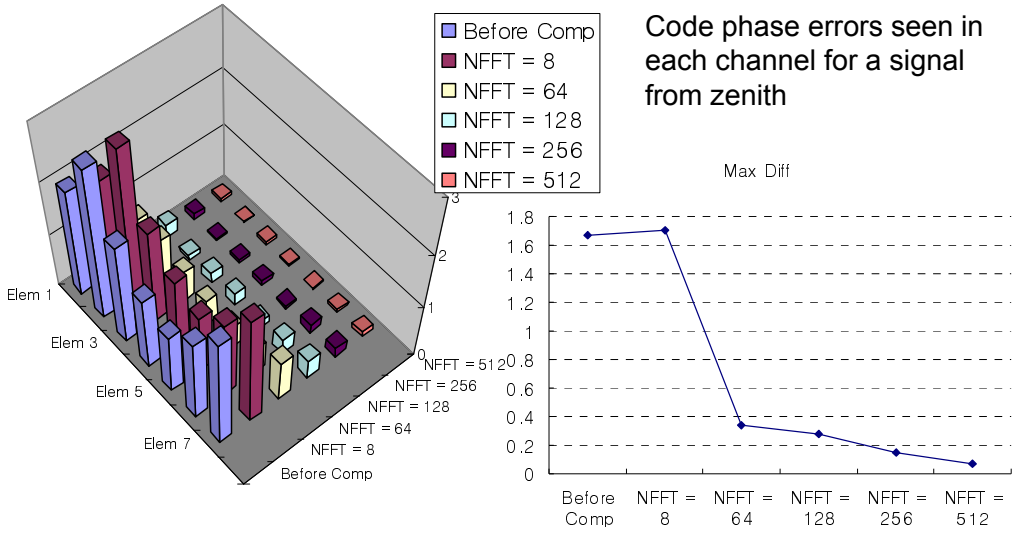

Figure 4-8. Channel Equalization Method Performance on Received Code Phase

Figure 4-8 above shows the ability of channel equalization in removing code phase errors in each antenna element channel of a seven element hexagonal array. For this computation, the incident signal arrives from the zenith direction, directly overhead. Thus, based on the geometry of the problem, all of the antenna elements should be receiving the same code phase. The fact that they are not is a result of mutual coupling between elements. NFFT refers to the number of FFT frequency bins used in the compensation. The 3-D plot on the left shows the received code phase errors versus perfect isotropic receiving elements in a CRPA array. The results are presented without any compensation and then with increasing levels of frequency bins in the channel equalization compensation. The plot

shows that eight frequency bins do not capture enough detail in the antenna frequency response to be able to undo the code phase errors. With more bins, the residual errors after compensation drop. The plot on the right helps us visualize this. Again, for a signal from zenith, the difference in received code phase between antenna elements should be zero. As we increase the number of frequency bins in the compensation, the antenna biases (including mutual coupling) are removed by the compensation scheme, and the maximum difference between two received code phases approaches zero.

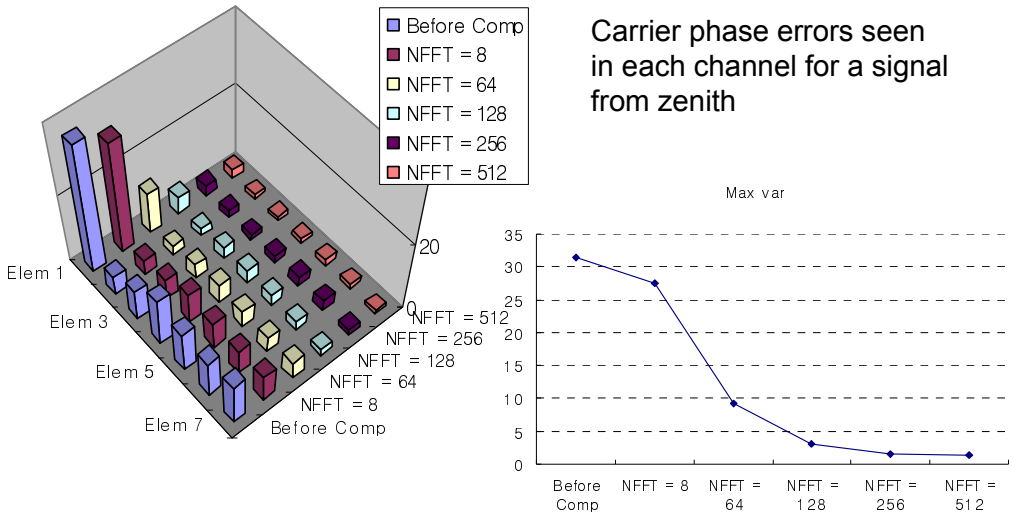

Figure 4-9. Channel Equalization Method Performance on Received Carrier Phase

Figure 4-9 presents the channel equalization results on the received carrier phase for antenna elements in a seven element hexagonal array. Again, this computation assumes

that the signal is incoming from the zenith, and ideal isotropic receiving elements should be receiving the same carrier phase. The uncompensated case on the left side plot shows significant variations. It is worth noting that the center element in the array (Element 1), which is surrounded on all sides by other elements and is thus impacted most by mutual coupling, shows the largest deviation in received carrier phase from the other elements. However, as was the case with code phase, increasing the number of frequency bins eventually eliminates the carrier phase error.

4.4 CHANNEL EQUALIZATION SCHEME COMPARISON TO CRPA POLYNOMIAL MODEL

As mentioned above, one of the benefits of using the channel equalization is that we have undone the antenna frequency effects upstream and we are left with nearly unbiased signals in each channel. Thus, we can choose a CRPA algorithm with the knowledge that hardware bias effects have been removed. This can be a great tool in investigating the amount of signal biases introduced by specific adaptive algorithms. Also, the frequency-based compensation lends itself nicely to be used in conjunction with

Spectral Frequency Adaptive Processing (SFAP) algorithms. If a SFAP algorithm can be developed to provide the RFI protection afforded by an adaptive process while at the same time minimizing additional unwanted signal biases, such an algorithm combined with the channel equalization scheme would be powerful for Sea based JPALS.

The pursuit of such an algorithm is an active topic of research at Stanford University and at other institutions involved with the JPALS program. For this dissertation, however, the channel equalization scheme will be combined with a deterministic beam-forming algorithm to produce a CRPA output signal. This protocol enables a meaningful comparison between the two compensation schemes presented in this chapter. Again, we will consider the sample constellation introduced in Section 3.5, which contains satellite pairs that are representative of possible worst case differential errors in both code and carrier phase for this CRPA system.

	Uncompensated CRPA Code Phase Error (m)	Code Phase Error w/ Equal. Comp (m) NFFT = 512	Code Phase Error w/ 6th model comp (m)	Uncompensated CRPA Carrier Phase Error (deg)	Carrier Phase Error w/ Equal. Comp (deg) NFFT = 512	Carrier Phase Error w/ 6th model comp (deg)
Max variation	1.36	0.043	0.020	40.1	1.2	5.0

Table 4-2. Compensation Scheme Residual Error Comparison

Starting with the code phase, the maximum residual code phase error variation seen for channel equalization with 512 frequency bins is 0.043 meters. This is slightly larger than the 0.02 meter residual error given by the sixth order polynomial model. Because the code phase data is used in the fit, the polynomial model is entirely inclusive of antenna frequency effects. The residual error that is seen for this method comes purely from fitting errors between the data and the model. However, for channel equalization, we are dealing with a finite number of frequency bins, and we cannot avoid some "discretization" effects as the antenna response data is compensated at the center frequency of each frequency bin. In other words, the continuous antenna frequency response cannot be perfectly modeled as a discrete function.

For the carrier phase, we see that the channel equalization actually does slightly better than the CRPA polynomial model. This is because for carrier phase, we are dealing with a single specific carrier frequency, and the "discretization" effect that affected the code phase response across the signal bandwidth is not so severe. The only error comes from slight mismatches between the carrier frequency and the center frequency of the closest frequency bin. As the number of frequency bins becomes larger, this mismatch will become smaller and smaller, approaching perfect carrier phase compensation. Whichever method we choose, the impact of CRPA biases on integer resolution is significantly mitigated.

4.5 COMPENSATION SCHEMES AND REAL WORLD APPLICATIONS

Two different compensation schemes were presented in this chapter that "bookend" the realm of possible compensation schemes. These schemes represent extremes in the hardware requirements for implementation and the amount of data that has to be carried by the receiver for compensation. The CRPA system polynomial model represents

the simplest scheme in terms of hardware and memory. However, it surrenders some RFI performance because it does not support adaptive CRPA processing.

The channel equalization method, however, will require a larger database of information to be carried. This database must contain magnitude and phase information in the specified number of frequency bins, over a given grid of incoming signal directions, for all of the antenna elements in an array. This becomes orders of magnitude more demanding on memory than the simple CRPA system polynomial model. For instance, a sixth order polynomial fit requires 49 coefficients each for code and carrier phase compensation for a total of 98 coefficients. For channel equalization, a minimum base requirement for modeling accuracy can be broken down as follows : 18 elevation points (5 degree increments) x 72 azimuth points (5 degree increments) x 256 frequency bins x 2 (magnitude and phase data required) = 663,552 data points. Although the current state of semiconductor technology shouldn't make the memory requirements for channel equalization prohibitive to implement, there is no denying that it is a much more expensive solution not only in terms of memory requirements, but also in terms of hardware implementation due to the use of FFT/IFFT modules.

The post-compensation errors quantified above are due to fitting error, discretization, or frequency mismatching. These models include all relevant antenna related characteristics, including the mutual coupling effects seen in an array. However, we have yet to take into account real-world considerations that are important for actual field implementation for Sea based JPALS. Some of these include environmental and manufacturing tolerance considerations, as well as logistical considerations such as unit-by-unit calibration. This will be the focus of the next chapter.

CHAPTER 5: COMPLETE ERROR BUDGETS

Chapter 3 of this dissertation focused on the code and carrier phase biases introduced by any CRPA. Chapter 4 described mitigation schemes to undo these biases. The data used in these earlier chapters were for a seven element hexagonal configuration using single probe fed rectangular patches designed and constructed for this research. The errors of interest so far have been discretization and fitting errors. In this chapter, we will extend our technical reach to investigate the real-world field implementation of a CRPA design to Sea based JPALS. This increase in scope will cause us to investigate other possible error sources. These include:

- Temperature variations (Section 5.2);
- Manufacturing tolerances of the antennas themselves (Section 5.3); and,
- Errors inherent in the data used to generate the compensation models (Section 5.4).

The antenna data for analysis and investigation in this chapter will come primarily from HFSS simulations. Sensitivity analyses, such as will be presented, are well suited to simulation studies, where we have full control over all antenna characteristics.

5.1 ERROR SOURCES IN EACH UNIQUE CRPA FIELD IMPLEMENTATION

Figure 5-1 lists the error sources that can propagate into uncompensated residual code and carrier phase errors, even if the mitigation schemes presented in the previous chapter are employed.

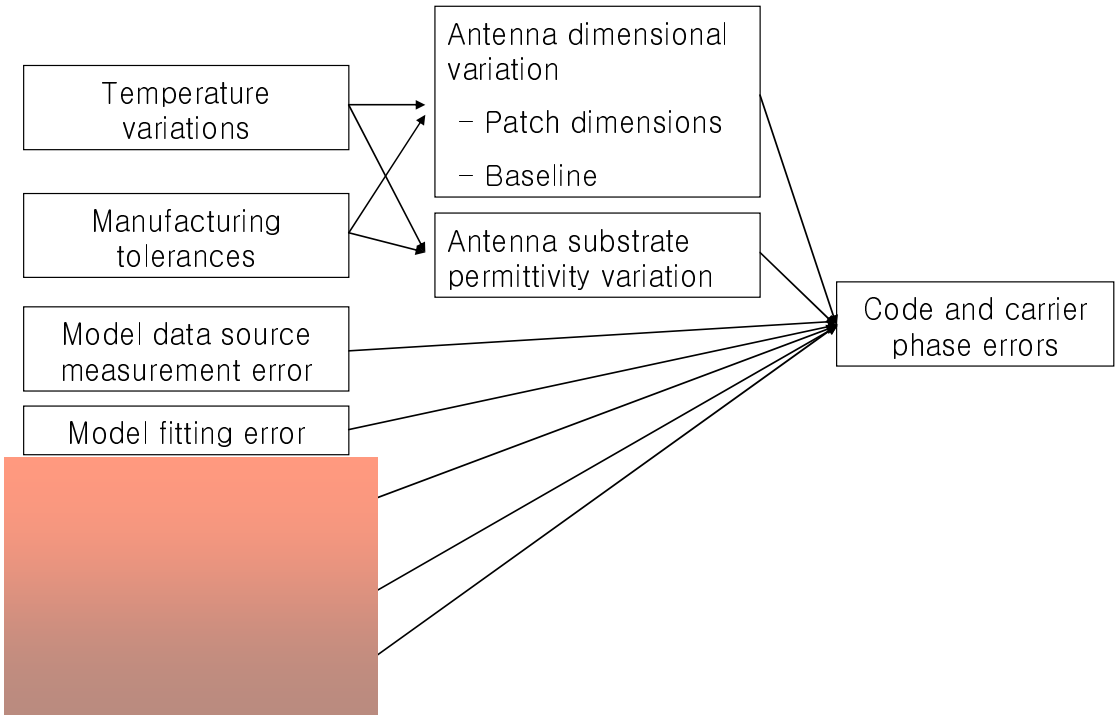

Figure 5-1. Possible Code and Carrier Phase Residual Error Sources for Case-by-Case Implementations of CRPA in Sea based JPALS

Temperature variations are due to the variable operating environment encountered by CRPAs within the Sea based JPALS application. Manufacturing tolerances are variations between individual antenna elements with in one CRPA as compared to other CRPAs from the same production line. Environmental errors and manufacturing errors manifest as code and carrier phase residual errors via identical means: dimensional variations in the antenna elements and the CRPA, and variations in the electrical material properties of the antenna substrate.

Model data source measurement error refers to errors in the data source used to generate the compensation models. This will arise from one of two sources, depending on which data set is used for model generation. For data from simulation, this error will include simulation noise, as well as any limitation of the simulation code in predicting actual antenna response. For data taken from the chamber, this error term will include measurement noise and test setup calibration errors. Model fitting errors are the polynomial fitting error and frequency resolution errors covered in Chapter 4.

The next three error sources shown in Figure 5-1 which are shaded out, are those that are specific to each CRPA environment. They are difficult to compensate for and add to the code and carrier phase errors in the compensated CRPA output. Ground plane variation refers to the different ground planes on which each CRPA is placed. The reference CRPA antenna will be located on the mast arm of the aircraft carrier island superstructure, and is more likely to have a standard ground plane. However, the CRPA located on the user platform will have a different aircraft body and structure for its ground plane. Multipath errors are entirely dependent on the antenna environment. There are currently some very interesting efforts to characterize and model the multipath environment

on an aircraft carrier, although at this stage the models are statistical [Weiss]. While these statistical models can provide good insight into the typical multipath environment seen on aircraft carriers, they are inadequate for predicting specific multipath errors in specific conditions. There is no doubt that the aircraft carrier is a very complicated environment for the reference antenna. Also, for the user antenna, the different tail structure of each aircraft, as well as surrounding environmental features all contribute to a unique multipath environment.

Radio frequency interference (RFI) will also add code and carrier phase errors to the compensated CRPA output signal. The CRPA will, of course, reduce the impact of RFI, but there will be some residual errors. As described earlier, our preferred CRPA algorithm is deterministic beam-forming because it does not introduce biases itself. However, it does not place nulls on the RFI sources either, and so an antenna gain pattern sidelobe may fall on the RFI source and errors will result. RFI will also persist when adaptive algorithms are used. While current adaptive algorithms can allow the user to operate in a harsher RFI environment, the algorithm itself will introduce some signal biases as a natural byproduct.

Again, these three error sources are case-by-case dependent and virtually impossible to estimate and bound. Thus, the tolerable code and carrier phase errors as presented in Chapters 1 and 2 have been decreased in order to provide margin for the additional errors introduced by multipath, noise, and RFI. Recall that the tolerable code and carrier phase errors are 8 cm and 10 degrees respectively. This chapter will focus on the first four error sources. A conservative bound will be placed on these error terms, and the sum of these error sources will be generated to determine if the integer ambiguity can be resolved. This will ultimately determine whether the compensated CRPA can be successfully implemented in a carrier phase differential GPS system like Sea-based JPALS.

5.2 TEMPERATURE EFFECTS

The material chosen in the antennas used in this research comes from the TMM® class of high frequency laminates from Rogers Corporation. The TMM® laminates are an ideal choice for this application due to their extremely stable thermal characteristics. These materials are widely used for GPS patch antennas. The material properties for the TMM 10 substrate material are given in Table 5-1

Properties	Typical Values	Applicable Condition
Dielectric Constant (ε_r)	9.2	10 GHz
Thermal Coefficient of ε_r	-38 ppm/K	-55 ~ 122 deg C
Thermal Expansion Coefficient	21 ppm/K (X-Y direction) 20 ppm/K (Z direction)	0~140 deg C

Table 5-1 Material Properties of TMM 10 Substrate Material [Rogers]

As shown, temperature affects the dielectric constant for the material as well as its dimensions. No other environmental effects are significant. The thermal expansion coefficients are close to that of copper (~17 ppm/K), which makes up the ground plane and the patch itself, so that the likelihood of "separation" between the substrate material and the copper cladding during temperature extremes is small.

For Sea-based JPALS, the operational environment encompasses all seasons, and all possible flight operations within a 50 nautical mile radius from the aircraft carrier [SRD]. This large broadcast radius for the differential data link supports all flight operations at all

altitudes, and is not limited to final approach and landing. Thus, we can imagine the operational flight altitude for Sea-based JPALS to span from sea-level up to 40,000 feet in both winter and summer months. A temperature variation from -40°C up to 60°C is certainly not unreasonable. On the low end, -40°C should be attainable in the winter months up in high altitudes. On the high end, 60°C should be a good high-end estimate as well during summer months with the array baking under direct sunlight within an enclosed dielectric radome, as is the case with current GAS-1 CRPA hardware. Thus, we consider a range of 100°C. This variation will affect the antenna in two ways: a change in the actual dielectric constant of the substrate material, and the actual physical expansion and contraction of the antenna dimensions. The applicable conditions given for the thermal coefficient of ε_r covers the operational temperature range we are considering. The applicable condition for the actual thermal expansion coefficients given in Table 5-1 does not cover our operational temperature range. However, given the lack of alternate data, and the fact that expansion coefficients should be smaller at lower temperatures, the values given in Table 5-1 will be used over our 100°C temperature range. This should yield a conservative bound on the expansion and contraction.

For a temperature range of 100°C, according to the coefficients given in Table 5-1, the impact range on the dielectric constant of the substrate is 0.0038 or ±0.0019. The impact of such a small dielectric constant variation is very small. A change in the dielectric constant of the substrate in effect shifts the center frequency of the antenna. From the rectangular patch antenna design derivation given in Chapter 2, we saw that the center frequency of the antenna has a 1/√ relationship with the dielectric constant. With such a small variation in the dielectric constant, we can expect to see a very small perturbation in the received carrier phase, and the frequency response of the antenna should be preserved. The only effect will be a slight decrease in antenna gain over the given bandwidth of the antenna.

Temperature will also affect the substrate dimensions. The expansion coefficients in Table 5-1 tell us that we can expect both the X-Y dimensions and the thickness of the patch to vary ±0.03 millimeters. This level of dimensional variation due to temperature will be investigated in conjunction with the manufacturing tolerance effects below, whose overall effect on the antenna's receiving characteristics manifest in similar fashion. The

handling of the two factors together should give us an overall view of receiving characteristic variations.

5.3 MANUFACTURING TOLERANCE

As with any product, manufacturing errors will exist and we must deal with dimensional tolerances in the manufacturing process. The antennas made for this research were constructed using high precision CNC milling machines, whose dimensional error tolerance is stated as ± 0.005 millimeters. However, one actual production using such CNC machines may be impractical in terms of time and cost. Unfortunately, all efforts to obtain actual dimensional tolerance specifications from patch antenna manufacturers were unsuccessful. Therefore, we will work with tolerance levels of current mass production circuit printing process capabilities which report tolerances ranging from as low as ± 0.01 millimeters for highly precise expensive solutions to ± 0.15 millimeters for inexpensive suppliers from China. We will take the high end value of this range, include the operational temperature range based dimensional tolerance of ± 0.03 millimeters, and add an inflation factor of about 10% to arrive at an overall dimensional tolerance of ± 0.2 millimeters. This

should be a good conservative estimate of overall variations that are possible between patch antenna elements fielded with the CRPA array. These variations will be investigated in a sensitivity analysis with normally distributed random variations. Normal distribution is an viable estimation of manufacturing dimensional variations [Miller].

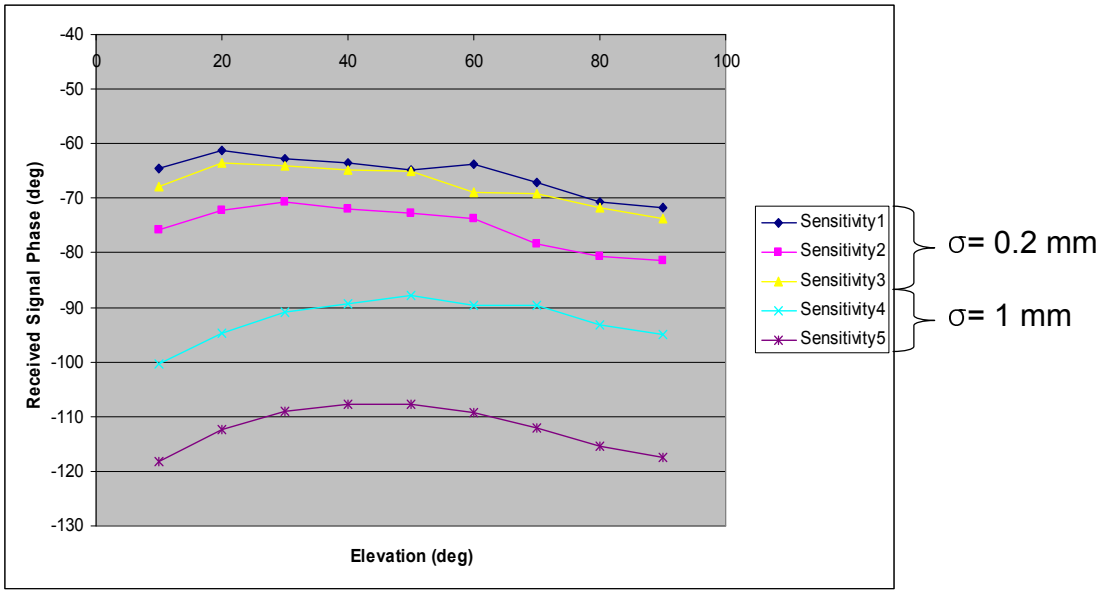

Figure 5-2. Received Carrier Phase Variation for Single Stand Alone Patch with Random Dimensional Variations (180 Azimuth Cut)

Figure 5-2 shows simulated received carrier phase sweeps over elevation for our reference patch antenna design. The different sensitivity trials have random variations in the X and Y axis dimensions, as well as in the thickness of the substrate and the location of the probe feed, all normally distributed with the σ values shown. While the received

carrier phase values do show significant variations between different dimensional tolerance study cases, the effect seems to be characterized by a constant offset, and the general pattern of the response over signal direction seems to be preserved. Figure 5-3 illustrates this point.

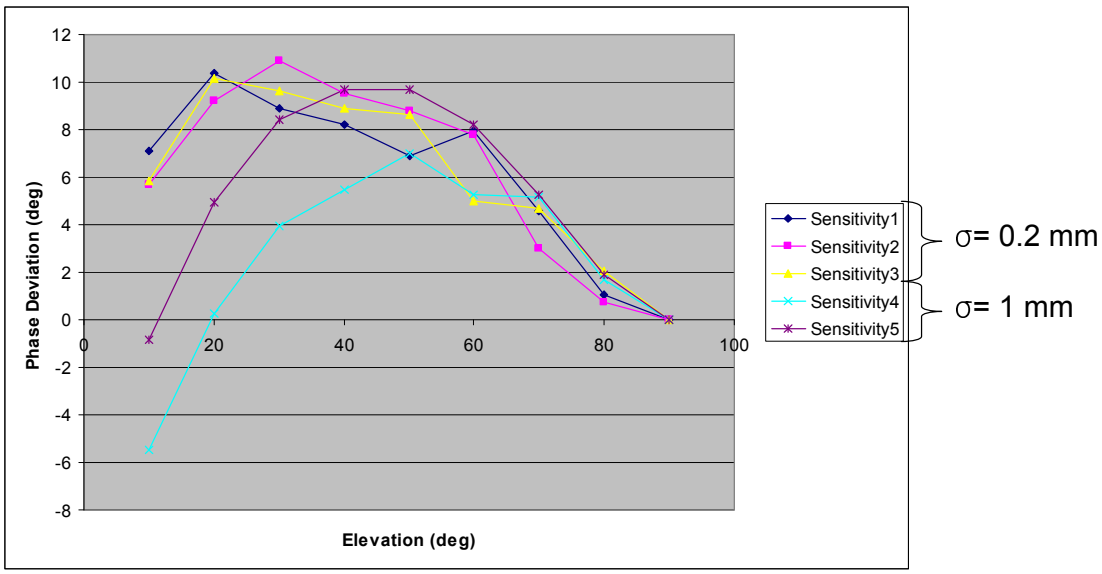

Figure 5-3. Received Carrier Phase Variation for Single Stand Alone Patch with Random Dimensional Variations (180 Azimuth Cut) with Constant Offset Bias Removed at Zenith

In Figure 5-3, the received phase exact offset value at zenith was removed for each curve to normalize to the first sensitivity trial. For the σ=0.2 mm cases, it is apparent that the shapes of the patterns are preserved within ±2 degrees of phase. Even for the exaggerated case of σ=1 mm variation cases, the pattern shape is relatively consistent

before it starts to deviate significantly at lower elevations. The constant offset characteristic can be attributed to the fact that variations of this magnitude cause only very small perturbations in the center frequency of the antenna such that the only recognizable effect is a constant bias. The general shape and features of the antenna are comparable enough to present a similar reception pattern over the incident signal directions.

Now the element to element spacing is considered. Not only will the individual antenna elements have different dimensional variations, there will also be a variation in the baseline locations of each antenna element. First, we'll just consider the effect that dimensional variation has on mutual coupling. Figure 5-4 shows the dimensional variation effect on a two element array configuration and the received carrier phase pattern of a patch antenna.

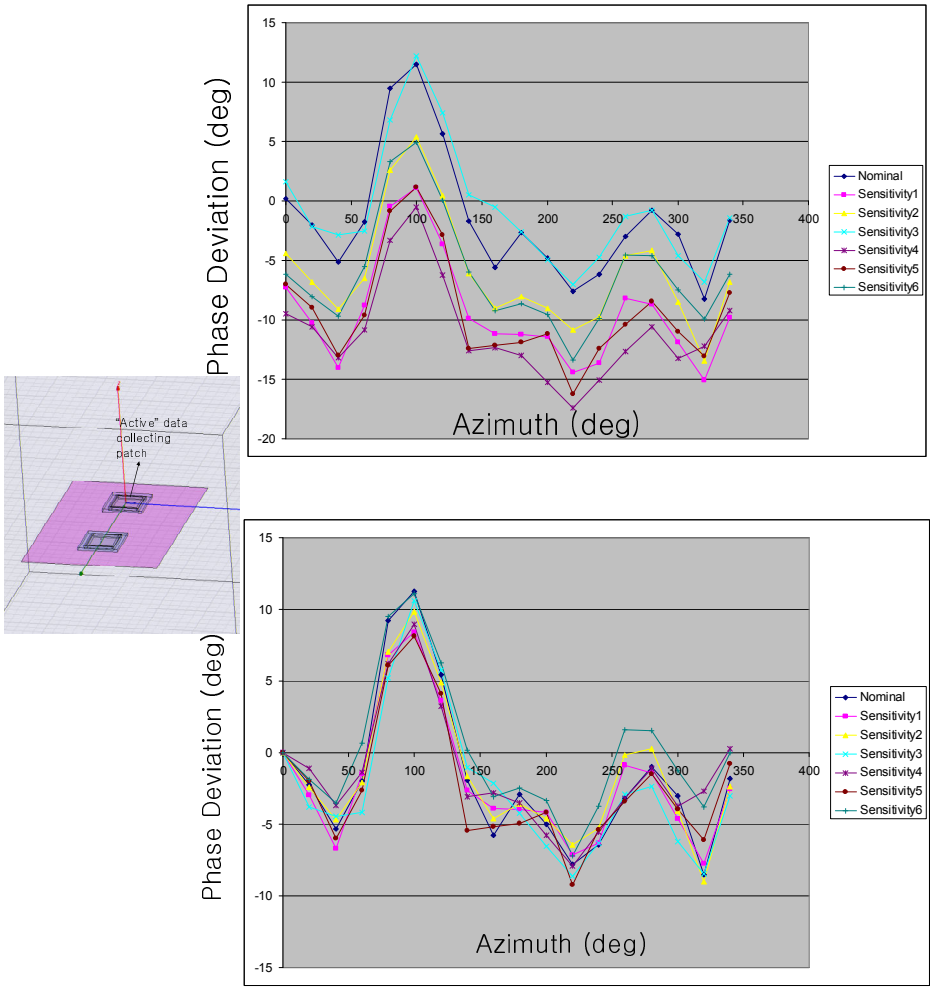

Figure 5-4. Dimensional Variation Effects on Mutual Coupling (2 Element Array)

The above figure shows the carrier phase effects of an antenna element's dimensional variation in a two element array for an azimuth sweep at 50 deg elevation. The data collecting patch (the antenna from which the phase measurements are read) is kept at nominal dimensions, while the second patch's dimensions are randomly varied, again

normally distributed with σ=0.2 mm. Thus, dimensional variation effect on mutual coupling is isolated. A similar trend can be seen for this case as was seen in the stand alone antenna case. Although we see some received phase differences, the effect seems to be a constant offset with little change in the pattern shape (top plot, Figure 5-4). Removing the constant offset values at 0 degree azimuth to collapse the patterns on top of each other verifies this observation (bottom plot, Figure 5-4). As can be clearly seen, the pattern shape is preserved to within $\pm$3 degrees of phase. The minor shifts in the center frequency of antenna elements in an array brought about by dimensional variation result in constant bias offsets in the mutually coupled carrier phase response.

One final dimensional variation to consider in CRPAs is the inter-element baseline variation. For this consideration, we will again use a random normally distributed dimensional variation with σ=1 millimeter, since we cannot expect circuit printing type accuracy for antenna element placement in an array (Figure 5-5). Again, the two element case investigated above will be presented with variations on the baseline length and location, while both antenna element dimensions are fixed at nominal.

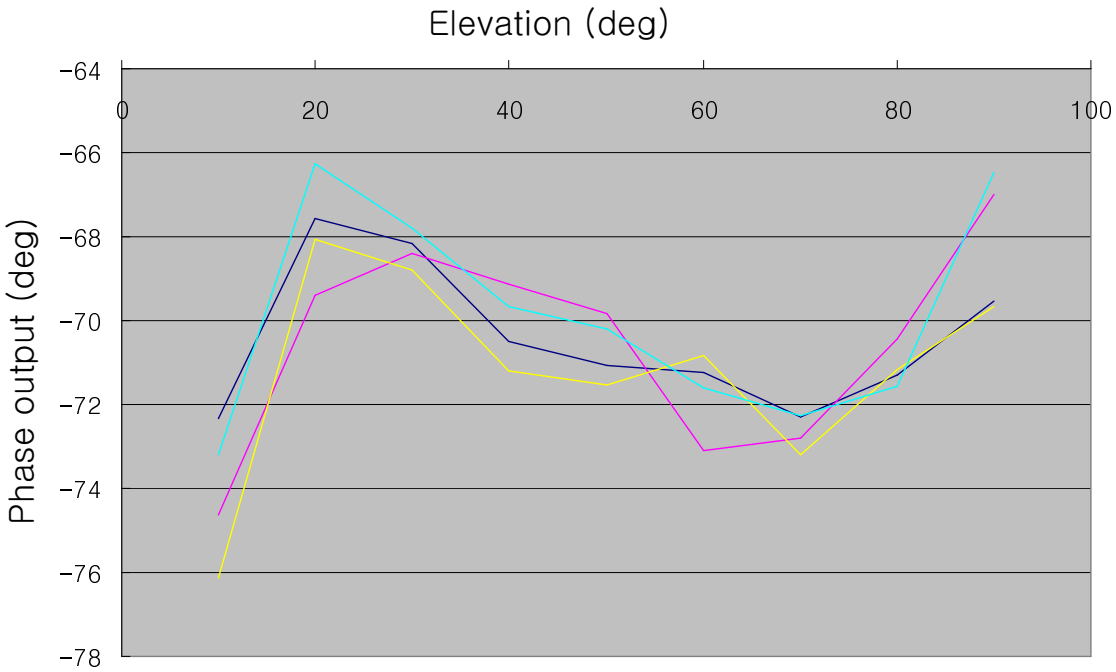

Figure 5-5. Dimensional Variation of Inter-Element Baseline (2 Element Array, Elevation Sweep at 0 degree Azimuth)

Figure 5-5 shows that baseline variations, even though we can expect larger variations than those on actual patch antenna dimensions, have less of an effect on the received carrier phase. The only effect is a variation of ±2 degrees or so with no other discernable effect. Combining the different dimensional variation effects presented above, and considering a worst case compounding of the variations, we can arrive at a conservative carrier phase dimensional variation error bound of ±5 degrees with the constant bias offset bound at 20 degrees.

5.4 MODEL DATA SOURCE MEASUREMENT ERROR

This error term captures errors in the data used to generate the compensation model. In other words, the model was generated using measurements with errors. This section focuses on errors in the data generation (simulation) or data collection (chamber) process.

Anechoic chamber measurements, when taken correctly, can be invaluable in characterizing antennas and their responses. However, special care must be taken in the chamber setup, and a thorough understanding of the chamber equipment is necessary to take chamber measurements as the definitive "truth." For example, one calibration issue that can add error is if the antenna under test is incorrectly mounted such that the center of rotation is not located at the feed point of the patch as the antenna is being rotated through its scans. In this case, the feed location will draw an arc as the antenna is rotated, and an artificial movement will be added in the antenna measurement. The anechoic chamber at Ohio University has an auto-calibration feature that removes this error. Another possible source of error here is measurement noise. The chamber used for this research provides 100 dB of noise isolation, minimizing the possibility of corrupting the scan data by introducing

colored noise from extraneous sources. This was verified when two separate scans were taken of an identical antenna at different times of the day and showed minimal phase variations (± 2 degrees).

For the case of simulation data sources, the magnitude of this error term will vary depending on the exact algorithms and methods used to generate the simulated results. Different simulation code packages employ different methods to simulate electrical structures. Any simplifications or assumptions that are made by the code package will manifest themselves as simulation errors. The simulation code package chosen for this dissertation, Ansoft's High Frequency Structure Simulator (HFSS), is a full 3D FEM field solver with an error-based iterative mesh generation algorithm. HFSS provides a trade between accuracy and simulation times. This trade can be controlled via the convergence criterion which has a bearing on the number of mesh elements generated in each simulation run. Simulation errors in HFSS will arise from the FEM approximations and the adaptive mesh seeding. This package, being a full solver of the Maxwell's equations which governs the relationship between electric and magnetic fields and currents, predicts patch antenna responses very well as will be shown below.

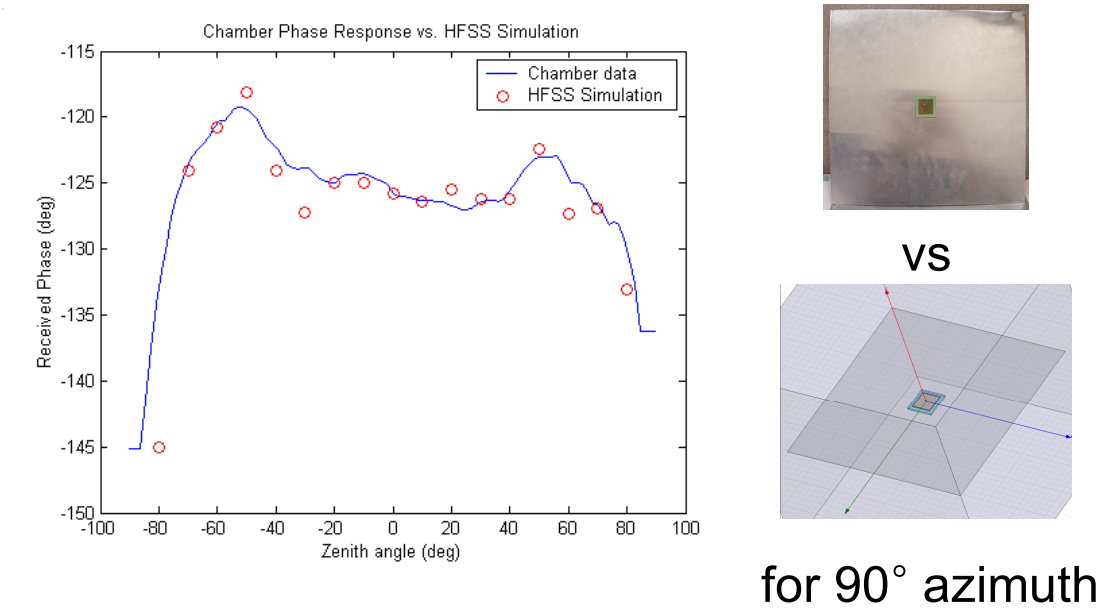

Figure 5-6 Chamber Measurements vs. Simulated Carrier Phase Response: Single Antenna

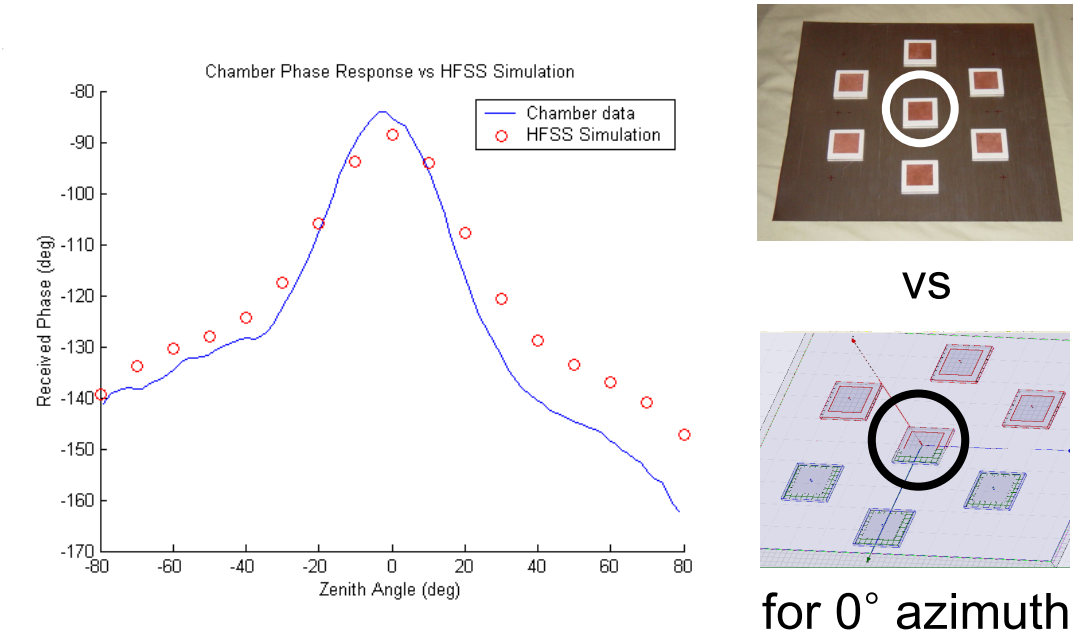

Figure 5-7 Chamber Measurements vs. Simulated Carrier Phase Response: 7 Element Array

The plots above show comparisons between the chamber measurement and the HFSS simulated response for our patch antenna design in both the stand alone configuration (Figure 5-6) and the seven element hexagonal array configuration (Figure 5-7). The simulated response predicts the chamber "truth" measurement quite well. The stand alone antenna comparison between chamber data and simulation data shows very close correlation. Even for the full seven element array case, the mutual coupling effects are captured well and the general trend of the phase response is predicted correctly.

The carrier phase errors arising from each source presented above are based on conservative educated estimates using the data in hand. For a more detailed consideration, enough data sets based on large sample sizes would be desirable to provide a full statistical analysis. However, with the limited amount of resources available in chamber time and with simulation run times not being conducive to generating multiple data sets, one must make do with conservative error bound estimates. Such a limitation is not only applicable to the research results presented here, but even more so for real world applications where chamber costs and time constraints can be more restrictive.

5.5 CODE PHASE CONSIDERATIONS

Thus far, error sources have been presented in the carrier phase only. The code phase analysis is much more challenging than the carrier phase analysis with respect to chamber costs and simulation time. A complete code phase consideration requires data sets over the bandwidth of interest with enough frequency resolution to capture the details of the frequency response variations. The amount of resources that were required to perform a full statistical analysis of the carrier phase based errors becomes orders of magnitude greater to perform for the code phase. The actual increase will depend on the frequency resolution that is chosen. From the channel equalization method discussion, at least 256 frequency bins are required to capture the antenna frequency response in enough detail.

Code phase consideration based on constant group delay measurements, while widely used and accepted in the general antenna community, is not adequate for the JPALS application. Constant group delay is a generalization that loses a lot of details that govern the code phase variations as covered in Chapters 2 and 3 (i.e., incident signal direction dependency, correlator spacing dependency, etc). Ironically, as mentioned in Chapter 2, the increased precision afforded by the higher bandwidth P(Y) coded signals, also has an

unwanted side impact in increased susceptibility to code phase variations, as compared to the lower bandwidth C/A coded signals. To illustrate this, let's go back and revisit Figure 2-8 reproduced below.

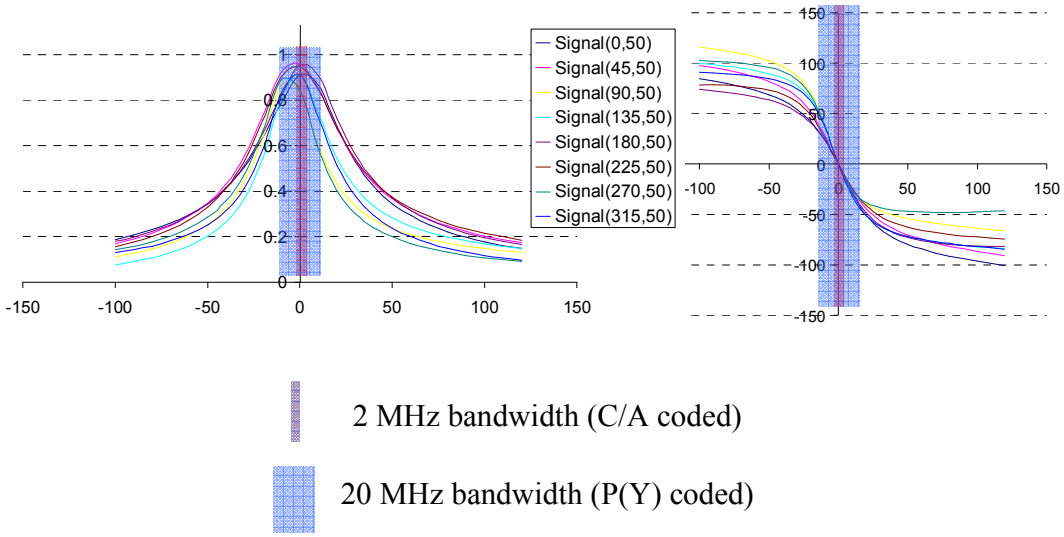

Figure 5-8. Antenna Gain and Phase Response vs. Frequency for Stand Alone Patch

As seen in the plot, over a 2 MHz C/A code bandwidth, there is virtually no variation in the carrier phase response versus incident signal direction. For the much wider 20 MHz P(Y) code bandwidth, the frequency variations are more pronounced. This leads to the P(Y) coded signals being more sensitive to dimensional variations, and their corresponding effects on the antenna frequency response, than a C/A coded counterpart.

Due to limited resources to perform a full statistical frequency content analysis, the code phase error bound will be placed in relation to the carrier phase error bound. A careful examination of the available data resulted in the following generalization. Given the exact dimensional perturbations used in some of the sensitivity trials presented in Figures 5-2, 5-3, and 5-4, the frequency content was simulated for a specified signal direction (60 degrees elevation, 180 degrees azimuth for stand alone case; 50 degrees elevation, 100 degrees azimuth for two element case), and the resulting code phase variation is presented in the table below.

	Carrier Phase error from nominal (constant bias offset removed)	% of overall nominal carrier phase variation range (~50 degree span)	Code Phase error from nominal	% of overall nominal code phase variation range (~80 cm span)
Sensitivity Trial 1 Stand alone	1.6 degrees	~3.2 %	1.2 cm	~1.5 %
Sensitivity Trial 2 Stand alone	1.8 degrees	~3.6 %	1.4 cm	~1.75 %
Sensitivity Trial 3 Stand alone	0.9 degrees	~1.8 %	0.7 cm	~0.9 %
Sensitivity Trial 4 2 element case	1.2 degrees	~2.4 %	1.1 cm	~1.4 %
Sensitivity Trial 5 2 element case	2.7 degrees	~5.4 %	2.1 cm	~2.6 %

Table 5-2. Code Phase Variation vs. Dimensional Sensitivity

The above table shows that the magnitudes of carrier phase dimensional variation and code phase dimensional variations seem to have some correlation. Closer investigation revealed that the ratios between the actual dimensional variation and the span of variation values over the visible hemisphere for the carrier and code phases have close to a 2:1

relationship (compare the third column to the fifth column). This generalized rule-of-thumb between the code and carrier phase errors holds for not only individual antenna dimensional variations, but also for mutual coupling variations in an array setting as well. Dimensional perturbation leads to the antenna element becoming slightly "mistuned" in its center frequency. This frequency "mistune" manifests immediately in the received carrier phase according to the $d\phi/d\omega$ slope. Code phase effects are not as direct. Code phase is affected not by the change in the received carrier phase value itself, but rather by the change in the shape of the frequency response (in both magnitude and phase). For the dimensional variation numbers we are dealing with, this frequency content effect is very subtle and can be approximated by the above rule-of-thumb. For example, using the above generalization, we arrive at code phase error bound for dimensional variation of ± 6 centimeters (approximately 10% of overall code phase variation span) based on the ± 5 degrees carrier phase variation error bound (approximately 20% of overall carrier phase variation span).

5.6 ERROR BOUND SUMMARY

Table 5-3 summarizes the carrier phase error budget for a CRPA implementation in Sea based JPALS with compensation. The numbers presented here are based on two assumptions. The model data source is taken to be the chamber measurements, and the compensation model is assumed to be the CRPA system polynomial fit model. The total sum of these error breakdowns presents a dreary picture (48 degrees).

However, there are two different calibration options that can be used to improve this result. First, if individual scans can be taken for all CRPA antennas coming off the manufacturing line to be used for model generation, the error budget in the entire grayed out box can be removed. Now, assuming these error budgets compound in worst case fashion, we are left with a total carrier phase error bound of 21 degrees. If the above is deemed to be too time consuming, a quicker smaller subset of scans can be made to just calibrate and remove the constant offset biases shown in the dark gray box. In that case, we are left with a total carrier phase error bound of 30 degrees.

	Temperature (-50°C ~ 50°C)		Manufacturing Tolerance		Measurement Error	Fitting Error
	Antenna Dimension Variation (Expansion)	Permittivity Variation	Antenna Dimension	Permittivity		
Carrier Phase Error : Constant Phase shift	5~7 deg	1~2 deg	8~12 deg	4~6 deg	< 3 deg (careful test setup should minimize this)	
Carrier Phase Error : Varition	2~4 deg	< 0.5 deg	4~6 deg	1~3 deg	2 deg	5 deg

Table 5-3. Error Bound Budget for CRPA Carrier Phase Bias Mitigation

Table 5-4 shows a similar breakdown for the code phase. The total code phase error bound can be placed at about 14 centimeters. Again, if a full scan can be performed in a chamber for each CRPA antenna coming off the manufacturing line, the grayed out terms can be removed and we are left with 5 centimeters of code phase error. Keep in mind that the chamber scans required to remove these gray box terms must include enough frequency content resolution to be able to form an accurate compensation manifold, and would take rather long to obtain.

	Temperature (-50°C ~ 50°C)		Manufacturing Tolerance		Measurement Error	Fitting Error
	Antenna Dimension Variation (Expansion)	Permittivity Variation	Antenna Dimension (< ±0.005")	Permittivity (< ±0.025)		
Code Phase Error	1~2 cm	< 1 cm	5~6 cm	2~3 cm	< 0.5 cm (careful test setup should minimize this)	2 cm

Table 5-4. Error Bound Budget for CRPA Code Phase Bias Mitigation

We are finally ready to fully evaluate the feasibility of CRPA use in Sea-based JPALS. As discussed earlier, CRPAs without compensation are unsuitable for differential carrier phase GPS. From the above analysis, results show that with a full calibration of each CRPA antenna fielded, code phase errors are bounded to approximately 4 centimeters and the carrier phase errors are bounded at approximately 20 degrees. Recall our requirement for code and carrier phase errors of 8 centimeters and 10 degrees respectively. We are within the requirement for the code phase error, but the carrier phase errors will be a problem. However, if we can have the CRPA antenna array temperature controlled, that will take away the possible environmental variations in Table 5-1. In that case, we will be left with a conservative carrier phase error bound of 10 degrees, and be able to successfully resolve the integer ambiguity problem.

For a partial calibration, which yields code and carrier phase error bounds of 14 centimeters and 30 degrees, or for general compensation without specific calibration, which yields 14 centimeters and 49 degrees of code and carrier phase error bounds, we are unable to resolve integers. Even with a temperature controlled CRPA array, the errors will be too large. The only thing we can do here is to take advantage of the second frequency signal at L2 and resort to wide lane processing. With dual frequency measurements, we can create a signal with a much longer wavelength (~86.2 cm). For this wide lane signal, the signal error requirements are much more relaxed, and the integers can be resolved even with the worst case errors mentioned above [Dogra].

CHAPTER 6: CONCLUSIONS

This dissertation presented an in depth analysis of the feasibility of using CRPA antennas for a carrier phase differential GPS system. Such an application has not been considered in previous work. To date, CRPA analysis has focused on RFI rejection alone. Sea-based JPALS needs RFI rejection and high integrity integer determination. JPALS is a dual-frequency carrier phase differential GPS system because it must provide navigation to support automatic landings onto aircraft carriers in zero visibility conditions. The system must have very tight accuracy requirements (0.2 meters in the vertical) and vertical alarm limits of 1.1 m. Thus, the dual frequency carrier phase differential GPS architecture is required.

The difficulty lies in that CRPAs and their algorithms in general leverage and modify the received signal in each antenna element channel before they are combined to form the CRPA output signal. This adjustment of the signal in each channel is what allows the CRPA system to change the receiving gain pattern of the array to suit the needs of each

particular application. Also the mutual coupling effects present within any array along with the frequency response variations over incident signal directions introduce biases in the CRPA output signal. Herein lies the problem. With any carrier phase differential GPS system, both the code and carrier phase must be measured accurately to facilitate the integer ambiguity resolution. CRPAs, while beneficial in providing RFI protection, make the integer ambiguity resolution problem difficult. The primary focus of this research has been to find a way to reap the benefits of CRPAs while minimizing the impact on carrier phase differential processing. This dissertation presented the following contributions:

- An analysis of the signal biases introduced by the CRPA antenna;
- Two representative mitigation schemes that compensate for the unwanted signal bias effects introduced by CRPAs;
- An analysis of environmental and manufacturing impact on the worrisome biases; and,
- A bound on the total error after CRPA compensation.

The above efforts were completed with the application to Sea-based JPALS in mind.

6.1 SIGNAL BIASES INTRODUCED BY CRPA ANTENNA ARRAY

Received signal characteristics on an individual patch antenna vary depending on the incident signal direction. In addition, individual antenna elements populated within a CRPA array do not behave as they would in a stand-alone case due to mutual coupling with the adjacent elements. The individual effects modified by mutual coupling propagate into the CRPA output signal and manifest as code and carrier phase biases.

In order to isolate the individual antenna element hardware effects and how these propagate down to the CRPA output, a simple deterministic beam-forming (DBF) algorithm was chosen. This algorithm was chosen specifically because it does not add any additional biases into the CRPA output signal, unlike current adaptive algorithms which alter the signal contents in each channel, thus injecting their own bias into the CRPA output.

The code and carrier phase variations over signal line-of-sight direction were presented for the above implementation. Carrier phase variations ranged over 40 degrees in total while the code phase variations ranged around 1.3 m. In the context of a differential system, this variation could manifest as a residual bias in the differenced signal. With the requirement for successful integer ambiguity resolution being placed at 8 cm and 10 degrees, it is readily apparent that the CRPA system, even with an algorithm that does not add any biases, is not suitable for use in Sea-based JPALS purely due to hardware bias effects.

6.2 SIGNAL BIAS MITIGATION FOR CRPAs

Two different mitigation schemes were introduced to compensate for the biases described above. The two schemes are the CRPA system polynomial and channel equalization. These two schemes bookend the spectrum of possible mitigation schemes in terms of implementation complexity and the amount of information storage required for carrying the models.

The CRPA system polynomial model was used in conjunction with a deterministic beam-forming (DBF) algorithm to characterize the CRPA output signal biases as a function of the azimuth and elevation angle of the line-of-sight direction. With that characterization, a least squares function fitting is performed on the CRPA output code and carrier phase data using polynomial base functions with azimuth and elevation as the variables. A sixth order polynomial function fitting requires 49 coefficients to be carried in memory to implement for each code and carrier phase model. This includes all cross product terms. With this model, the maximum possible fitting errors remaining in the differenced signal after compensation (i.e., fitting errors) are 2 centimeters and 5 degrees for the code and carrier phase, respectively. The benefit of this scheme is the simplicity in implementation. The model generated corrections can be made as an adjustment in the tracking loops of the GPS receiver that processes the CRPA output signal. Also, the amount of information required to carry this model is very modest. The only drawback is that we are constrained to the DBF algorithm which is not the most effective of the CRPA algorithms in RFI protection. However, for this application, it is prudent to exchange some RFI protection for a gain in signal integrity.

The channel equalization scheme undoes the antenna frequency response effects in each channel via an FFT/IFFT pair module. With the antenna hardware effects undone in each channel before complex weighting, we are free to choose any CRPA algorithm with the knowledge that most of the biases have been removed. A cost effective implementation of this scheme would pair this scheme with a SFAP algorithm, which can take advantage of the FFT/IFFT modules in place to share the FFT hardware requirements. This would give great flexibility to deal with a variety of different challenging RFI scenarios. However, current SFAP algorithms are not constrained to avoid introducing additional biases from the SFAP algorithm. Importantly, the number of frequency bins used in the compensations must be high enough to capture the details of the antenna frequency response. For comparison purposes to the CRPA polynomial model, channel equalization with 512 frequency bins was deterministically beam-formed to gauge the residual biases in the CRPA output signal. The residual code and carrier phase biases remaining in the differenced signal after this compensation scheme was 4.3 centimeters and 1.2 degrees in code and carrier phase respectively.

6.3 TOTAL SYSTEM ERROR BOUND FOR A COMPENSATED CRPA

Real world implementations of CRPAs must consider several error sources beyond the fitting error summarized above. The operating temperature range of JPALS along with the thermal material properties of the substrate and patch materials contribute to the amount of received code and carrier phase variations that we will see with our designed patch antenna. Manufacturing tolerances which result in dimensional variation and substrate permittivity variation between CRPA antenna hardware samples will similarly lead to received signal variations.

The compensation models can be generated using the following three different implementations. They have been listed in order of decreasing complexity and required calibration time.

1. A full calibration of each CRPA antenna coming off the manufacturing line for all incident signal directions: The corresponding model fit to that calibration data will remove manufacturing tolerance related variations.

2. A simpler shorter calibration procedure in one given signal direction: Only the constant offset bias seen in the carrier phase response due to manufacturing variation is removed.

3. No calibration: The compensation model will be based off a general data set, and the manufacturing tolerance related variations will manifest as residual errors in the compensated CRPA output signal.

Of course, there can be errors inherent in the data set used to generate the models themselves, but careful set up and the right equipment should minimize this error source. The total system error bound should include the model fitting errors as well.

Error sources that are entirely dependent on the application environment that cannot be modeled or confidently bounded include ground plane variations, multipath errors, and RFI induced errors. These error terms must be tolerated, and thus, it behooves us to try to reach as small a known error as possible to allow margin for the above unknowns.

	Worst case error w/ no compensation	Worst case error for compensation w/ no calibration scan	Worst case error for compensation w/ simple calibration scan	Worst case error for compensation w/ full calibration scan	Worst case error for compensation w/ full calibration scan and temperature controlled array
Code Phase	~150 cm	~14 cm	~14 cm	~4 cm	~2.5 cm
Carrier Phase	~ 100 deg	~49 deg	~30 deg	~20 deg	~10 deg

Table 6-1. Total CRPA System Error Bound Assuming Sixth Order CRPA System Polynomial Model Compensation Using Chamber Data Fit Model

Table 6-1 summarizes the total CRPA system error in both code and carrier phase, assuming compensation of antenna hardware biases using the sixth order polynomial model based on chamber data. Comparing the above results to the requirements we had for successful integer ambiguity resolution (~8 centimeters and ~10 degrees in code and carrier phase), full calibration of each CRPA antenna should allow us to resolve integers if we use temperature controlled CRPA arrays. However, for both the partial calibration and no calibration of each CRPA antenna, we must fall back to the wide-lane signal to start our integer ambiguity resolution.

6.4 FUTURE WORK

CRPAs and their application to a carrier phase based system such as Sea-based JPALS is a rich field of research. In the future, the analysis and methods presented in this dissertation should be extended to cover the dual frequency stacked patch antenna array. This is a challenging topic, because the two stacked patches interact with each other and complicate the coupling between stacks. Another antenna based future research topic would be the pursuit of further antenna improvements (increased bandwidth, optimum patch geometry, 3D arrays, etc).

The community should also seek an adaptive CRPA algorithm that minimizes the code and carrier biases. This is a current subject of research both at Stanford University and at other institutions closely involved with the JPALS program. Once achieved, this will allow greater RFI protection while still allowing carrier phase differential processing for the utmost accuracy and precision.

Sea-based JPALS presents a daunting challenge. This program is a multi-institutional, multi-disciplinary effort that will draw on the most advanced of technologies and the keenest minds in the industry. Other advanced topics such as ultra- deep INS-GPS

integration and advanced dual frequency carrier phase differential positioning are concurrently being pursued, and it will be a great achievement when these disciplines come together to field this ambitious product.

BIBLIOGRAPHY

[Allen] B.Allen, M.Ghavami. *Adaptive Array Systems: Fundamentals and Applications,* Wiley, 2005

[Balanis] C.Balanis. *Antenna Theory: Analysis and Design,* Wiley-Interscience 3rd ed., 2005

[Bartone] C.Bartone. "EECS/AEC Antenna Anechoic Chamber," Facility Specifications and Introduction Document, Ohio University Avionics Engineering Center, 2005

[Bauer] F.H.Bauer *et al* "The GPS Space Service Volume," Proceedings of Institute of Navigation GNSS 06, 2006

[Behre] C.Behre *et al* "A Comparison of Measured Jamming Mitigation Performance from Field Tests with Predictions from Hardware-Based CRPA Simulations and Analytic Simulations," Proceedings of Institute of Navigation GPS 02, 2002

[De Lorenzo 04] D.De Lorenzo *et al* "GPS Attitude Determination for a JPALS Testbed: Integer Initialization and Testing," Proceedings of IEEE Position Location and Navigation Symposium 04, 2004

[De Lorenzo 06] D. De Lorenzo *et al* "Navigation Accuracy and Interference Rejection for an Adaptive GPS Antenna Array," Proceedings of Institute of Navigation GNSS 06, 2006

[Dogra] S.Dogra *et al* "Sea-Based JPALS Relative Navigation Algorithm Development," Proceedings of Institute of Navigation GNSS 05, 2005

[Enge] P.Enge, P.Misra. *Global Positioning System : Signals, Measurements, and Performance,* Ganga-Jamuna Press, 2001

[Godara] L.Godara. *Smart Antennas,* CRC, 2004

[Hein] G.Hein, W.Werner. "Comparison of Different On-The-Fly Ambiguity Resolution Techniques," Proceedings of Institute of Navigation GPS 95, 1995

[James] J.R.James, P.S.Hall. *Handbook of Microstrip Antennas,* INSPEC Inc, 1998

[Kaplan] D.Kaplan, C.Hegarty. *Understanding GPS: Principles and Applications*, Artech House Publishers 2nd edition, 2005

[Kim 04] U.Kim *et al* "Phase Effects Analysis of Patch Antenna CRPAs for JPALS," Proceedings of Institute of Navigation GNSS 04, 2004

[Kim 05] U.Kim *et al* "Analysis of Carrier Phase and Group Delay Biases Introduced by CRPA Hardware," Proceedings of Institute of Navigation GNSS 05, 2005

[Manolakis] D.Manolakis, V.Ingle, S.Kogon. *Statistical and Adaptive Signal Processing: Spectral Estimation, Signal Modeling, Adaptive Filtering and Array Processing*, Artech House Publishers, 2005

[McGraw] G.McGraw *et al* "Assessment of GPS Anti-Jam System Pseudorange and Carrier Phase Measurement Error Effects," Proceedings of Institute of Navigation GNSS 05, 2005

[Miller] S.R.Miller. "Statistical tolerance in the framework of concurrent engineering," Reliability and Maintainability Computer-Aided Engineering in Concurrent Engineering, 1990 and 1991., Combined Proceedings of the 1990 and 1991 Leesburg Workshops, 1991

[Monzingo] R.Monzingo, T.Miller. *Introduction to Adaptive Arrays*, SciTech Publishing, 2003

[Parkinson] B.Parkinson, J.Spilker. *Global Positioning System : Theory and Application*, American Institute of Aeronautics and Astronautics, 1996

[Pervan 01] B.Pervan, F.C.Chan. “System Concepts for Cycle Ambiguity Resolution and Verification for Aircraft Carrier Landings,” Proceedings of Institute of Navigation GPS 01, 2001

[Pervan 03] B.Pervan *et al* “Performance Analysis of Carrier-Phase DGPS Navigation for Shipboard Landing of Aircraft,” Navigation Journal vol. 50 no.3, The Institute of Navigation, 2003

[Peterson 04] B.Peterson *et al* “Feasible Architectures for Joint Precision Approach and Landing System (JPALS) for Land and Sea,” Proceedings of Institute of Navigation GNSS 04, 2004

[Peterson 05] B.Peterson *et al* “Investigation of Common Architectures for Land- and Sea-Based JPALS,” Proceedings of Institute of Navigation GNSS 05, 2005

[Rogers] “TMM Temperature Stable Microwave Laminate Data Sheet,” Product Specifications and Material Properties for Rogers TMM Class Substrate Material

[Rounds] S.Rounds. “Jamming Protection of GPS Receivers,” GPS World, February 2004

[SRD] “System Requirements Document for SRGPS,” R2 Baseline v1.0, August 2003

[Stutzman] W.Stutzman, G.Thiele. *Antenna Theory and Design*, Wiley 2nd ed., 1997

[Swanson] D.Swanson. "Microwave Circuit Modeling Using Electromagnetic Field Simulation," Artech House Publishers, 2003

[Teunissen] P.J.G.Teunissen *et al* "The Volume of the GPS Ambiguity Search Space and its Relevance for Integer Ambiguity Resolution," Proceedings of Institute of Navigation GPS 96, 1996

[Visser] H.Visser. *Array and Phased Array Antenna Basics,* Wiley, 2005

[Weiss] J.P.Weiss *et al* "Aircraft Carrier Multipath Modeling for Sea-Based JPALS," Proceedings of Institute of Navigation GNSS 05, 2005

[Widrow] B.Widrow, S.Stearns. *Adaptive Signal Processing*, Prentice Hall, 1995

[Zurcher] J.F. Zurcher. *Broadband Patch Antennas*, Artech House Publishers, 1995